FZK-370
15 June 1970

# DEVELOPMENT OF A SMALL INTEGRATING TISSUE EQUIVALENT QUARTZ FIBER ELECTROMETER DOSIMETER



NUCLEAR AEROSPACE RESEARCH FACILITY

operated by

GENERAL DYNAMICS
Fort Worth Division

FZK-370

NUCLEAR AEROSPACE RESEARCH FACILITY

15 June 1970

# DEVELOPMENT OF A SMALL INTEGRATING TISSUE EQUIVALENT QUARTZ FIBER ELECTROMETER DOSIMETER

C. S. Sims

**Prepared for the Manned Spacecraft Center National Aeronautics and Space Administration Houston, Texas**

Contract No. NAS 9-8752

GENERAL DYNAMICS
*Fort Worth Division*

## ABSTRACT

A quartz fiber electrometer dosimeter system has been designed, developed, and tested to demonstrate the applicability of small dosimeters of the Neher type for use as space qualified instruments. The electrometer consists of a quartz rod 30 mm long and 3 mm in diameter partially coated with Au, and a 10 micron diameter quartz fiber coated with Signa-Kote to a resistance between 0.25 and 1.5 megohm/cm. The tissue equivalent ionization chamber has a volume of 9 cc, is filled with 1 atm. of ethylene, and consists of the automatic recycling quartz fiber electrometer inside a 112 mg/cm$^2$ Signa-Kote coated Delrin electrode and a 103 mg/cm$^2$ Al case. Eight design verification units with various electrometer properties were tested to determine their operating characteristics. The optimum operating voltage for these dosimeters ranged from 30 to 100 volts. The dosimeters were calibrated using $^{60}$Co at several dose rates extending over 5 orders of magnitude and the response was quite good. The temperature effects on the units, investigated over intervals as large as 220°F (i.e. -40 to +180), do not present any cause for concern. Simulated mission vibration and shock testing did not alter the detection characteristics of the unit tested. Additional tests concerning orientation in gravity fields and gas leakage were also generally satisfactory. The work was performed for the Manned Spacecraft Center, National Aeronautics and Space Administration, Houston, Texas under Contract No. NAS 9-8752.

TABLE OF CONTENTS

TABLE OF CONTENTS (Cont'd)

TABLE OF CONTENTS (Cont'd)

LIST OF FIGURES

LIST OF FIGURES (Cont'd)

LIST OF TABLES

# I. INTRODUCTION

## 1.1 Background Information

Before dealing directly with the quartz fiber electrometer dosimeter system, it is of interest to consider some supporting information.

### 1.1.1 History of the Use of Quartz Fibers in Radiation Dosimetry

Quartz fibers have been used in instruments for radiation detection and dosimetry for more than 3 decades. Several of these uses are presented in Table 1-1.

Table 1-1 Use of Quartz Fibers in Radiation Detection and Dosimetry

| Year | Investigator(s) | Instrument | Ref. No. |
|---|---|---|---|
| 1937 | C. C. and Thomas Lauritsen | pocket chamber type with scale viewed through eyepiece | 1 |
| 1953 | H. V. Neher | automatic recharging ionization chamber | 2 |
| 1956 | H. V. Neher and Alan R. Johnston | modified automatic recharging ionization chamber | 3 |
| 1961 | H. V. Neher | variable sensitivity automatic recharging ionization chamber | 4 |
| 1964 | Rolf Hosemann and Harold F.H. Warrikhoff | self-powered gamma ray dosimeter | 5 |
| 1967 | R. J. Adams | high pressure proportional counter | 6 |

There exists in the literature additional work describing techniques of construction[7] and application[8] of some of the instruments mentioned in Table 1-1.

### 1.1.2 Another Application of Quartz Fibers

There are many areas of science in which the use of quartz fibers has led to the development of excellent instruments. One of these areas is the accurate weighing of objects with extremely small masses. In 1948, Kirk and Schaffer[9] constructed quartz fiber helical balances in connection with their biological studies. Their design was improved upon by Drew and Ernsberger[10] in 1953. These balances were very good, but in 1969 Hemenway and Patashnick[11] developed a new and much more sensitive microbalance. In connection with micrometeorite research, they produced an instrument that will directly measure masses in the range $10^{-5}$ - $10^{-11}$ grams and, with modification, will provide even greater sensitivity.

### 1.1.3 Working with Quartz Fibers

Building instruments utilizing quartz fibers requires knowledge of the properties and behavior of quartz as well as experience with the physical manipulation of it. There exist problems, such as the consistent pulling of very small diameter fibers and the preservation of these fibers once they are obtained, which may not have obvious solutions to the observer. There is no substitute for experience in areas like these, but a study of proven methods and techniques is valuable. Properties of quartz, procedures for working

working with it, its cleaning, care, and preservation have been discussed in the literature by Neher[12] and by Craig and Kirk.[13]

### 1.1.4 Application to Space Radiation Dosimetry

In 1965, a commercially obtained quartz fiber electrometer (QFE) assembly* was evaluated[14] by GDFW to determine its applicability for use in a small, lightweight, integrating dosimeter system operating on the principle of Neher's instrument.[2] That investigation revealed that many problems exist with a system of the desired type. Some of these problems involve sensitivity, reproductibility, temperature and vibration stability, and the erratic recharging of the coated quartz rod anode. In spite of the problems involved, it was indicated that the concept should be worth trying in a dosimeter for manned space flight.

## 1.2 Nature and Objectives of the Present Task

The Fort Worth Division of General Dynamics Corporation performed the work under Contract NAS 9-8752.

### 1.2.1 General Scope of the Effort

The purpose of this work was to design, construct, and evaluate a small automatic recycling QFE dosimeter and to define its applicability for use as a space qualified instrument. The work is recognized as preliminary, but it is a vital step forward in the evolution of a

---

*The assemblies were obtained from Electro-Optical Systems, Inc., Pasadena, California. EOS no longer manufactures or markets electrometer assemblies of the type tested.

first-line QFE dosimeter system.

### 1.2.2 Details of the Effort

The statement of the general scope of the work is broad, therefore, clarifying detail is presented in the following discussion.

#### 1.2.2.1 The Dosimeter

The dosimeter is to be an instrument of the Neher type.[2] The requirement that it be lightweight and small means that the entire dosimeter must be much smaller than Neher's instruments and, consequently, the QFE assemblies must be much smaller than those tested by GDFW[14] in 1965. This also differs from the 1965 effort, which evaluated only the QFE assembly, in that a tissue-equivalent ionization chamber operating on the Bragg-Gray principle must house the QFE assembly.

#### 1.2.2.2 The Evaluation Tests

These tests are designed specifically to determine whether or not the dosimeter is qualified for space flight. They include determining the dosimeter response at various dose rates and temperatures using various sources as well as performing mission vibration simulation and shock tests.

Calibration and testing with alpha, beta, gamma, and proton radiation will necessarily be performed on space qualified QFE dosimeter systems developed using the experience gained during this work, but the evaluation tests described herein include only those using gamma sources.

## II. THEORETICAL CONSIDERATIONS

Theoretical considerations are vital to any scientific endeavor. They give direction to experiment and serve as a basis from which to better understand the phenomena being observed. The development of relationships pertaining to the QFE assembly as well as the QFE dosimeter system are presented in this Section.

In order that those unfamiliar with instruments of this type might be able to follow through the ensuing discussion, the operation of the QFE dosimeters is briefly explained. A quartz fiber and a quartz rod are both coated so as to be electrically conducting and placed within a tissue equivalent ionization chamber (TEIC). The fiber is placed in tension against the rod. When voltage is applied to the fiber, the assembly is charged and the fiber is repelled from the rod by the Coulomb repulsive force. As the charge on the rod is reduced by the radiation, the tension in the fiber returns it to the rod and the cycle is repeated. The pulse created during each cycle will be the indication that a predetermined amount of radiation has been absorbed in the walls of the TEIC.

The QFE action may take place in a manner different from that just described. Consider a coated quartz fiber placed a very small distance away from a coated quartz rod. A voltage is applied to the fiber from a battery, the other side of which is connected to the ionization chamber case. The rod, acting as the anode, collects charge as the chamber gas is ionized. When enough charge of opposite sign to the

fiber charged is collected, the fiber will move under the Coulomb attractive force, recharge the rod, and return to its position away from the rod. The cycle is then repeated. This method is referred to as the NC (for fiber Not originally in Contact with the rod) method. The theoretical considerations presented herein will deal directly with the "regular" method described first, but the results are applicable to both types of QFE units.

## 2.1 Force and Deflection Calculations for the QFE Assembly

The equations and calculations for the Coulomb force between the coated rod and fiber as well as for the resulting fiber deflection are derived and presented in the subsequent discussion.

### 2.1.1 Earth Gravity Force on Fiber

The gravity force on the quartz fiber is calculated below:

$F_g$ = gravity force on quartz fiber, dynes

m = mass of the fiber, grams

L = fiber length, cm

$d_f$ = fiber diameter, cm

p = fiber density = 2.2 grams/cc

g = acceleration of gravity = 980.665 cm/sec$^2$

$$F_g = mg = \pi\left(\frac{d_f}{2}\right)^2 Lpg. \qquad (1)$$

When the known values are used, Equation 1 becomes

$$F_g = 1694.4\ d_f^2 L. \qquad (2)$$

This force as a function of L for various diameters is shown in Figure 2-1.

2.1.2 Repulsion Force Between Rod and Fiber

It is of interest to make an approximate calculation of the repulsion force between the fiber and the rod of the QFE units. Following the definitions and Figure 2-2, that calculation is shown.

$F_r$ = Coulomb repulsive force, dynes

$\sigma$ = #coulombs/cm on fiber

$\lambda$ = #coulombs on rod

$L_e$ = length of electrical conductor coated portion of quartz rod, cm

y = rod radius, cm

r, x, c, d = lengths, cm (refer to Figure 2-2)

L = fiber length = c + d, cm

Gauss' law may be written as

$$EA = \frac{Q}{\epsilon_o} \qquad (3)$$

where E is the electrical field, A the area of concern, Q the charge, and $\epsilon_o$ the proportionality constant. The surface area of the cylindrical portion of interest at radius r is

$$A = 2\pi r L_e. \qquad (4)$$

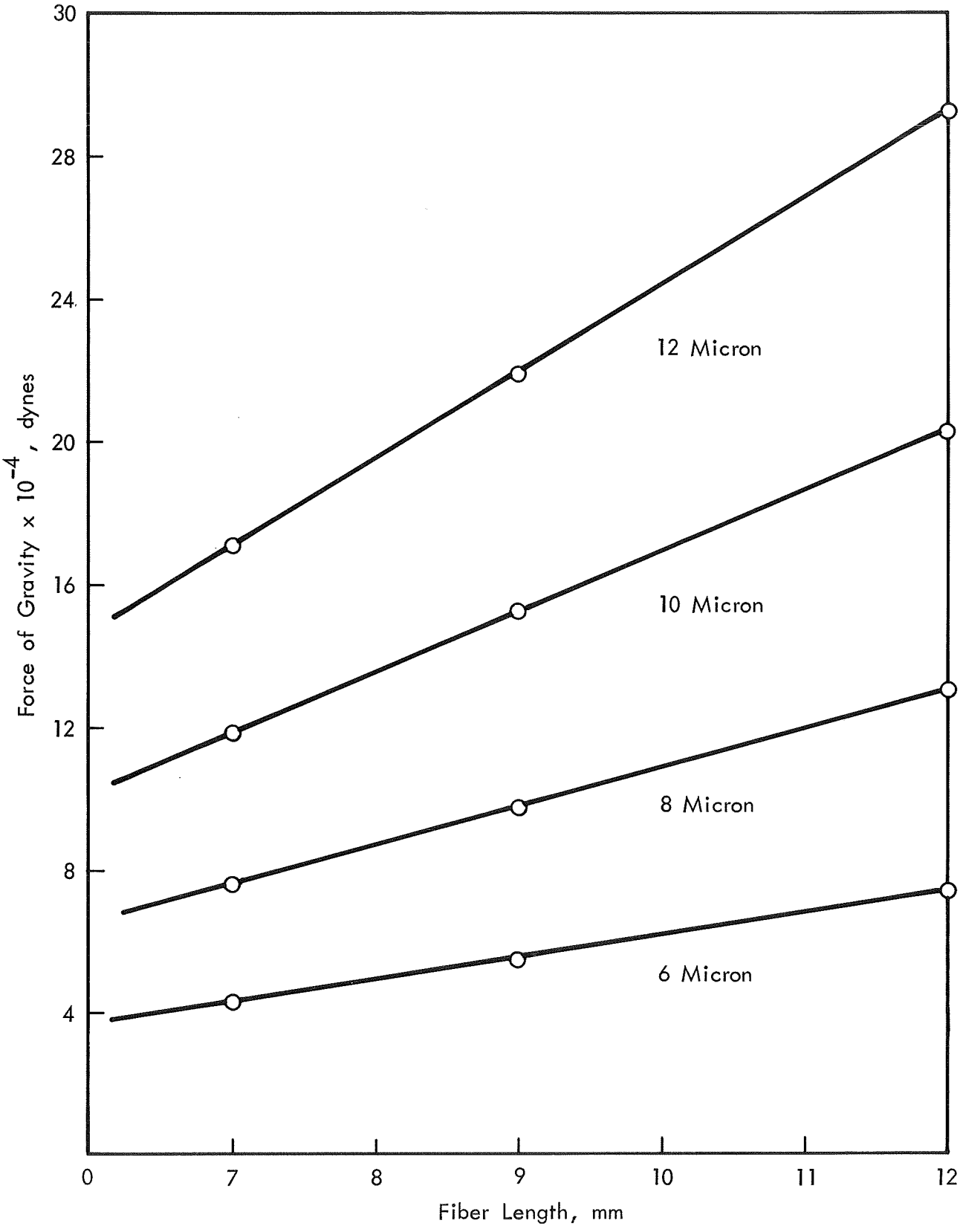


Figure 2-1 Gravitational Force vs. Fiber Length for Various Diameter Fibers

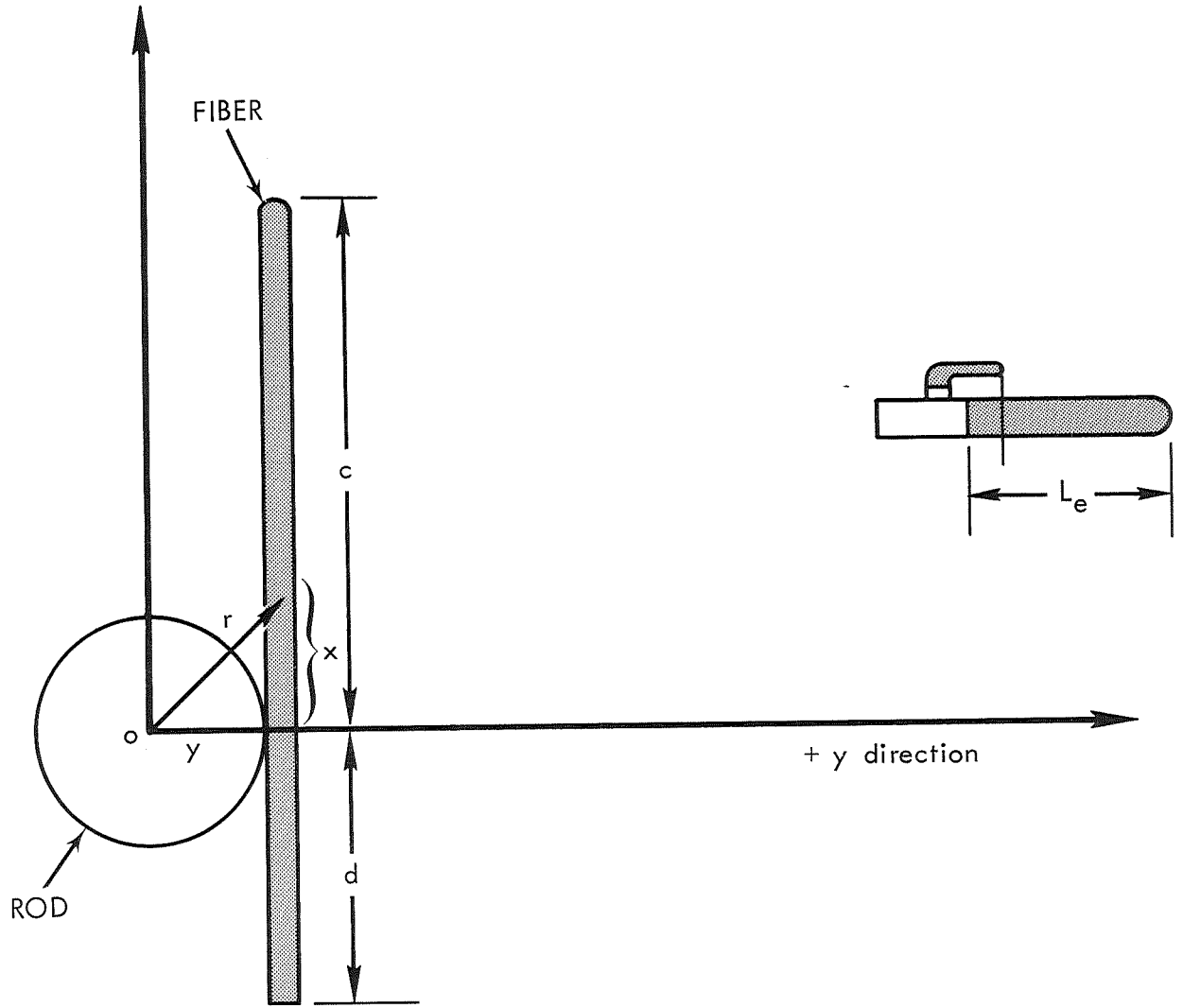


Figure 2-2 Schematic of QFE Assembly for Calculational Use

Combining Equations 3 and 4 and using the definitions above, the following equation is obtained.

$$E(r) = \frac{Q}{\epsilon_o A} = \frac{\lambda}{2\pi\epsilon_o r L_e} \tag{5}$$

In general, the force on a charged body placed in the field described by Equation 5 is given by

$$F_r = \int E(r)\, dq \tag{6}$$

where dq is the differential charge on the body. In our problem, dq is the differential charge on the conducting fiber and may be written as

$$dq = \sigma\, dx. \tag{7}$$

Using Equations 5 and 7, 6 becomes

$$F_r = \frac{\lambda\sigma}{2\pi\epsilon_o L_e} \int_x \frac{dx}{(x^2+y^2)^{1/2}} \tag{8}$$

where $r^2 = x^2+y^2$. Using $\epsilon_o = 8.87\ (10^{-17})$ and inserting the integration limits, Equation 8 becomes

$$F_r = 17.98(10^{14})\ \frac{\sigma\lambda}{L_e}\left(\int_o^c \frac{dx}{(x^2+y^2)^{1/2}} + \int_o^d \frac{dx}{(x^2+y^2)^{1/2}}\right). \tag{9}$$

After performing the indicated integration, Equation (9) becomes

$$F_r = 17.98(10^{14}) \frac{\sigma\lambda}{L_e} \left( \ln \left[ \frac{c + \sqrt{c^2+y^2}}{y} \right] + \ln \left[ \frac{d + \sqrt{d^2+y^2}}{y} \right] \right) \quad (10)$$

which is the approximate expression for the Coulomb repulsive force between the rod and the fiber.

2.1.3 Moment of Inertia

The moment of inertia of a circular cross section of a rod is

$$I = \frac{\pi r^4}{4} \quad (11)$$

about the axis passing through the center of gravity of the rod. When the quartz fiber is considered, Equation 11 becomes

$$I = \frac{\pi d_f^4}{64} \ cm^4 \quad (12)$$

where $d_f$ is the fiber diameter.

2.1.4 Young's Modulus for Small Diameter Quartz Fibers

A least squares curve fit was performed on available data and an equation for Young's modulus was determined for small diameter quartz fibers. The fitted curve, shown in Figure 2-3, is given by

$$Y = 7\ (10^{11}) + \frac{13\ (10^7)}{d_f} \quad dynes/cm^2. \quad (13)$$

2.1.5 Deflection of the Fiber

The deflection of the fiber away from the rod may be calculated by solving the basic equation

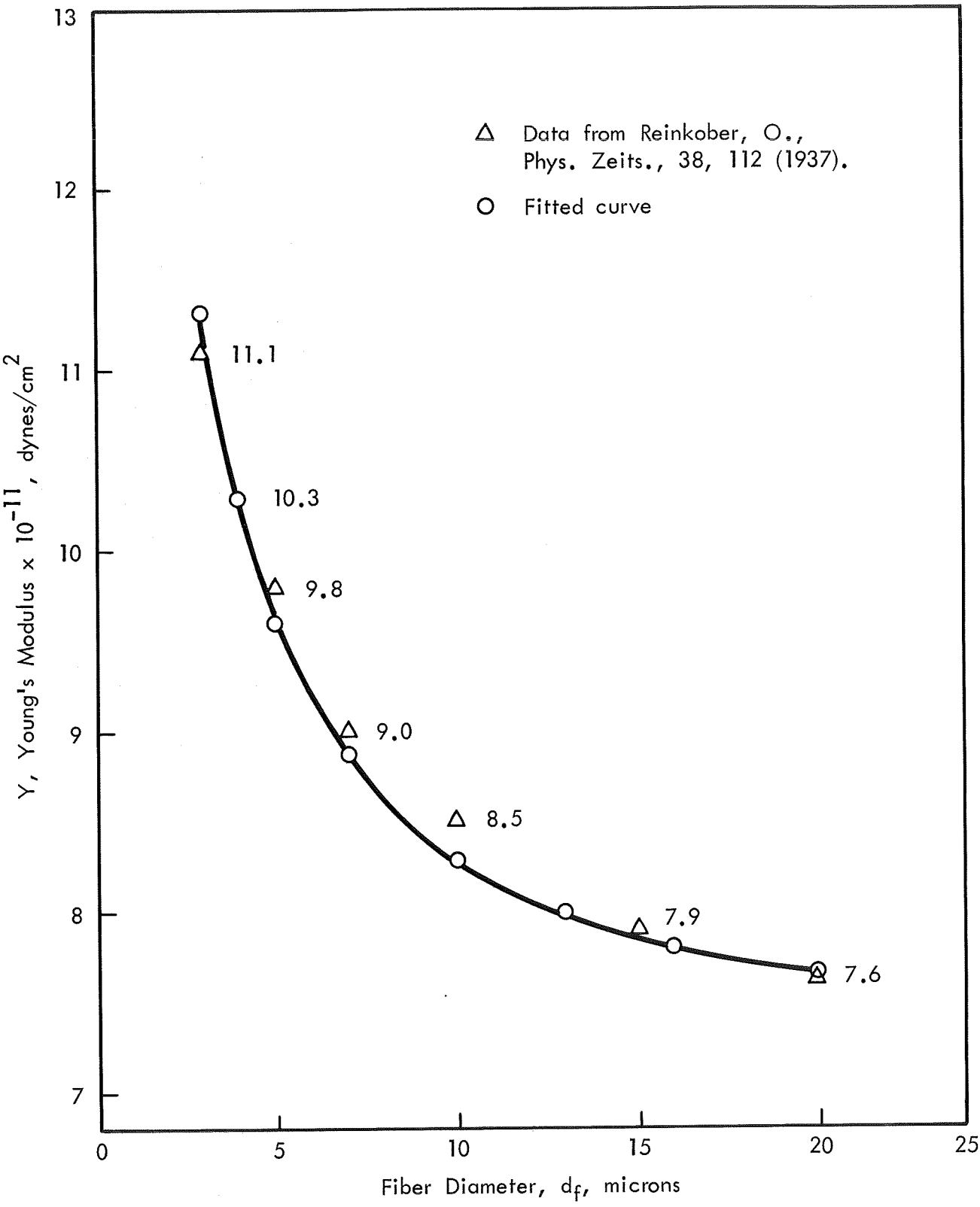


Figure 2-3 Curve Fitted to Elastic Modulus Data

$$YI \frac{d^2s}{dx^2} = -M_x \tag{14}$$

where s is the displacement of the fiber from its original position, in cm, and $M_x$ is the bending moment. Y and I have previously been defined. It is assumed that the repulsive force, $F_r$, acts at the center of mass. The system is shown in Figure 2-4.

From consideration of the free body diagram, it is seen that

$$P_a = F_r \tag{15}$$

and

$$M_a = -F_r\frac{L}{2}. \tag{16}$$

Then, for $0 \leq x \leq \frac{L}{2}$,

$$M_x = -F_r\frac{L}{2} + F_r x = F_r(x - L/2). \tag{17}$$

For $\frac{L}{2} \leq x \leq L$,

$$M_x = -F_r\frac{L}{2} + F_r x - F_r(x - L/2) = 0. \tag{18}$$

Equation 14 must thus be solved for the two values of $M_x$ as defined by Equations 17 and 18. They are written as Equations 19 and 22 and are solved below.

$\underline{0 \leq x \leq \frac{L}{2}}$

$$YI\frac{d^2s}{dx^2} = F_r\,(L/2-x) \tag{19}$$

$$x = 0;\ s = \frac{ds}{dx} = 0$$

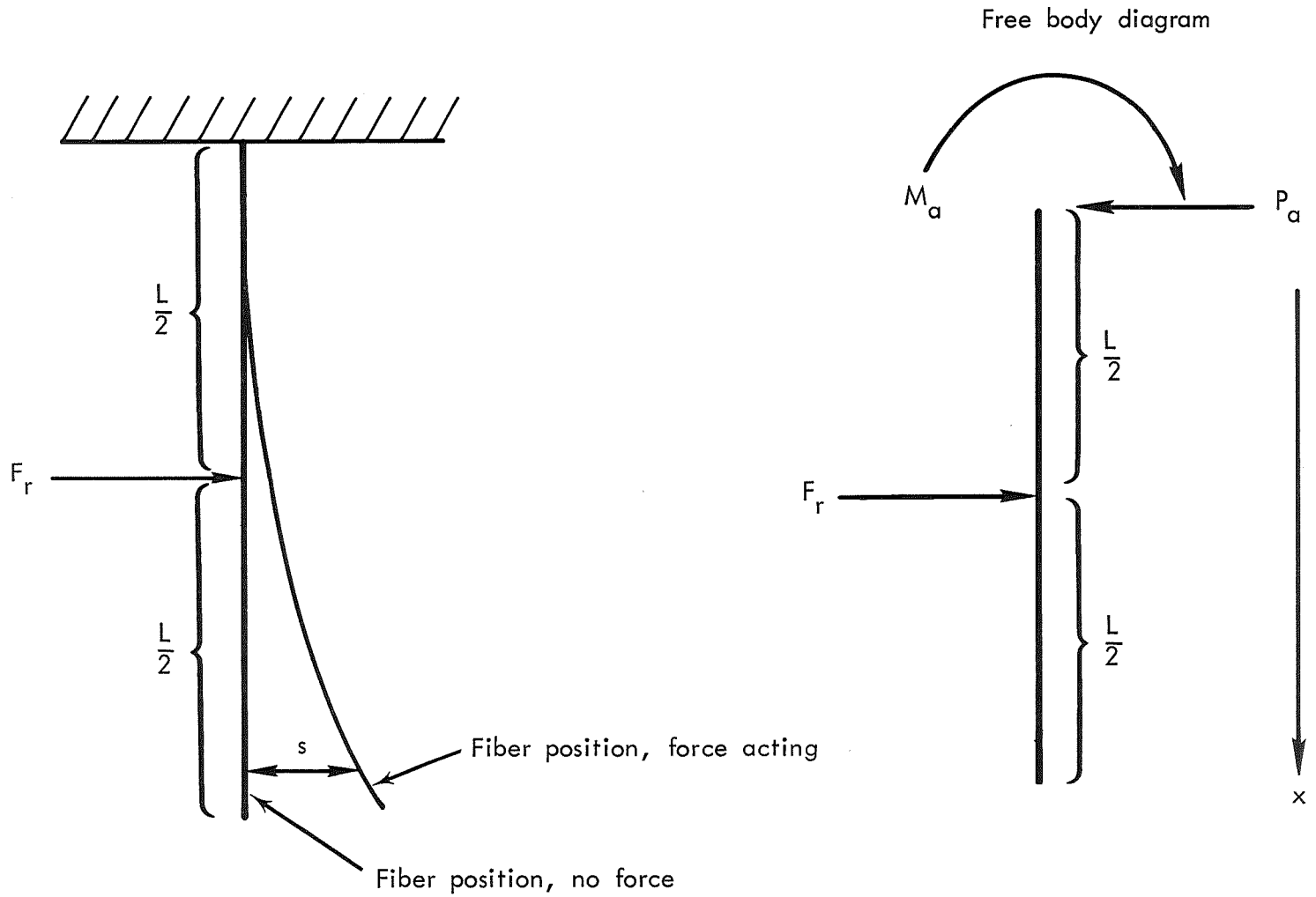


Figure 2-4 Schematics for Deflection Calculations

$$YI \frac{ds}{dx} = \frac{F_r x}{2} (L - x) \tag{20}$$

$$s = \frac{F_r x^2}{2YI} \left( \frac{L}{2} - \frac{x}{3} \right) \tag{21}$$

$\frac{L}{2} \leq x \leq L$

$$YI \frac{d^2 s}{dx^2} = 0 \tag{22}$$

$$x = \frac{L}{2} \; ; \; s = s \text{ (Eq. 21)}, \; \frac{ds}{dx} = \frac{ds}{dx} \text{ (Eq. 20)}$$

$$YI \frac{ds}{dx} = \frac{F_r L^2}{8} \tag{23}$$

$$s = \frac{F_r L^2}{8\ YI} (x - L/6) \tag{24}$$

The force, $F_r$, is said to act at the center of mass (cm) of the fiber in a radial direction. The displacement in the y direction (see Figure 2-2) is caused by the component of $F_r$ in that direction, i.e., $F_y$. $F_y$ is given by

$$F_y = F_r \ (y/r)_{cm} \tag{25}$$

where

$$r_{cm} = \sqrt{x_{cm}^2 + y^2} \tag{26}$$

and

$$x_{cm} = \frac{1}{2}(c-d) \tag{27}$$

Using the above, Equations 21 and 24 become

$$s = \frac{F_y x^2}{2\ YI} \quad (L/2 - x/3), \quad 0 \le x \le L/2 \tag{28}$$

and

$$s = \frac{F_y L^2}{8\ YI} \quad (x - L/6), \quad L/2 \le x \le L. \tag{29}$$

2.1.6 Computation Results

Computations made utilizing the relationships developed in the preceding 5 portions are shown here.

2.1.6.1 Force Calculations

One of the requirements for successful operation of the QFE in various gravitational fields is that the repulsive force between the rod and fiber be greater than the force of gravity on the fiber. It is assumed that the earth's field will be the largest in which sustained operation will be required. Figure 2-5 shows the relative size of these forces for various sized fibers.

The repulsive force itself is very dependent on the amount of charge on the rod and the charge per unit length on the fiber. This force is plotted against the charge product in Figure 2-6 for two rod sizes. The larger rod shows a smaller force of repulsion for the same charge due to the fact that the average distance between the concentrations of charge is greater.

2.1.6.2 Deflection Calculations

The displacement of the fiber from its original position is shown in Figure 2-7 for two fibers of different diameter subjected

to the same force. Figure 2-8 shows the displacement of 10 micron diameter fibers subjected to various forces.

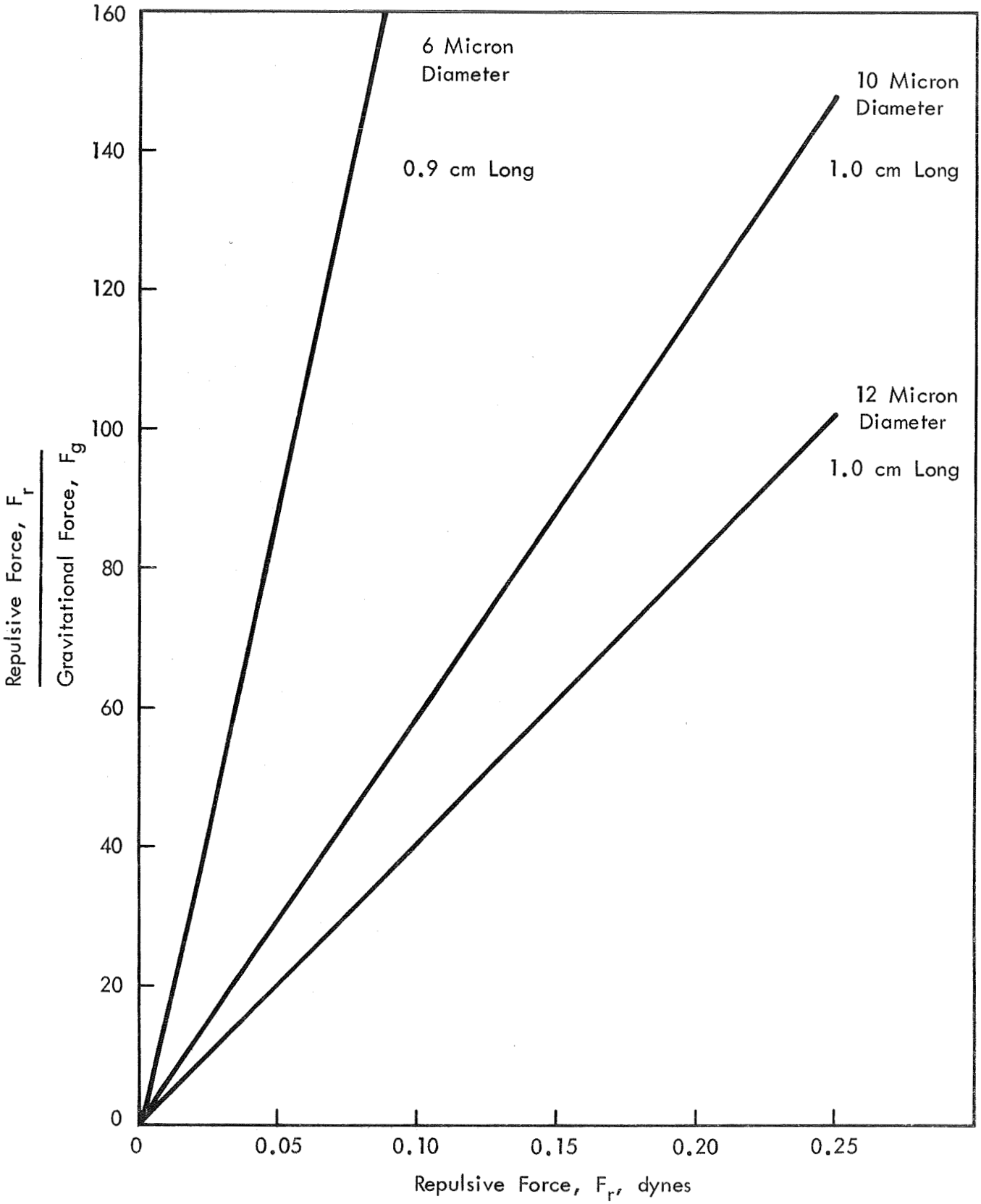


Figure 2-5 Comparison of the Repulsive and Gravitational Forces

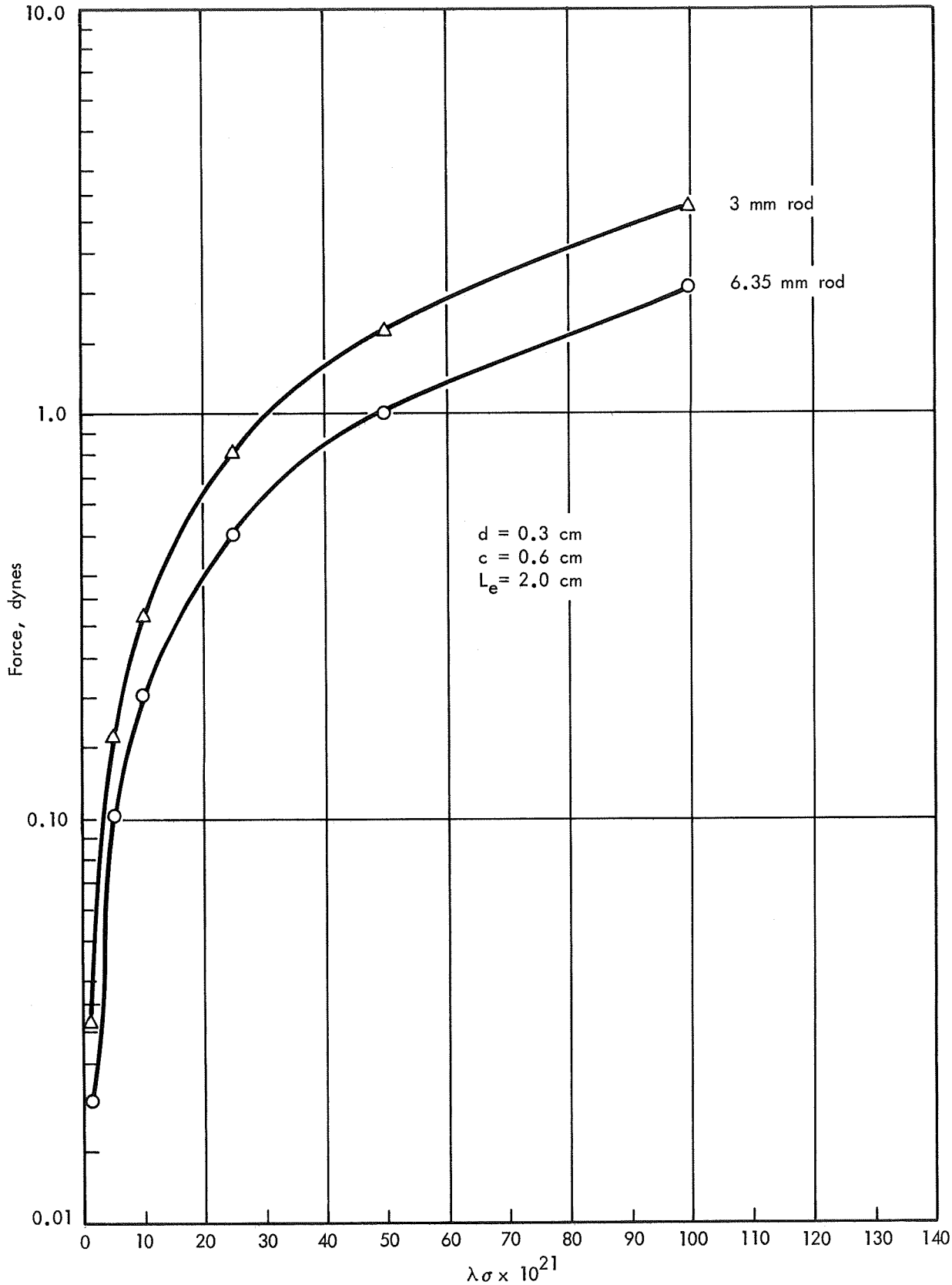


Figure 2-6 Force vs. Charge Product with Rod Daimeter as Parameter

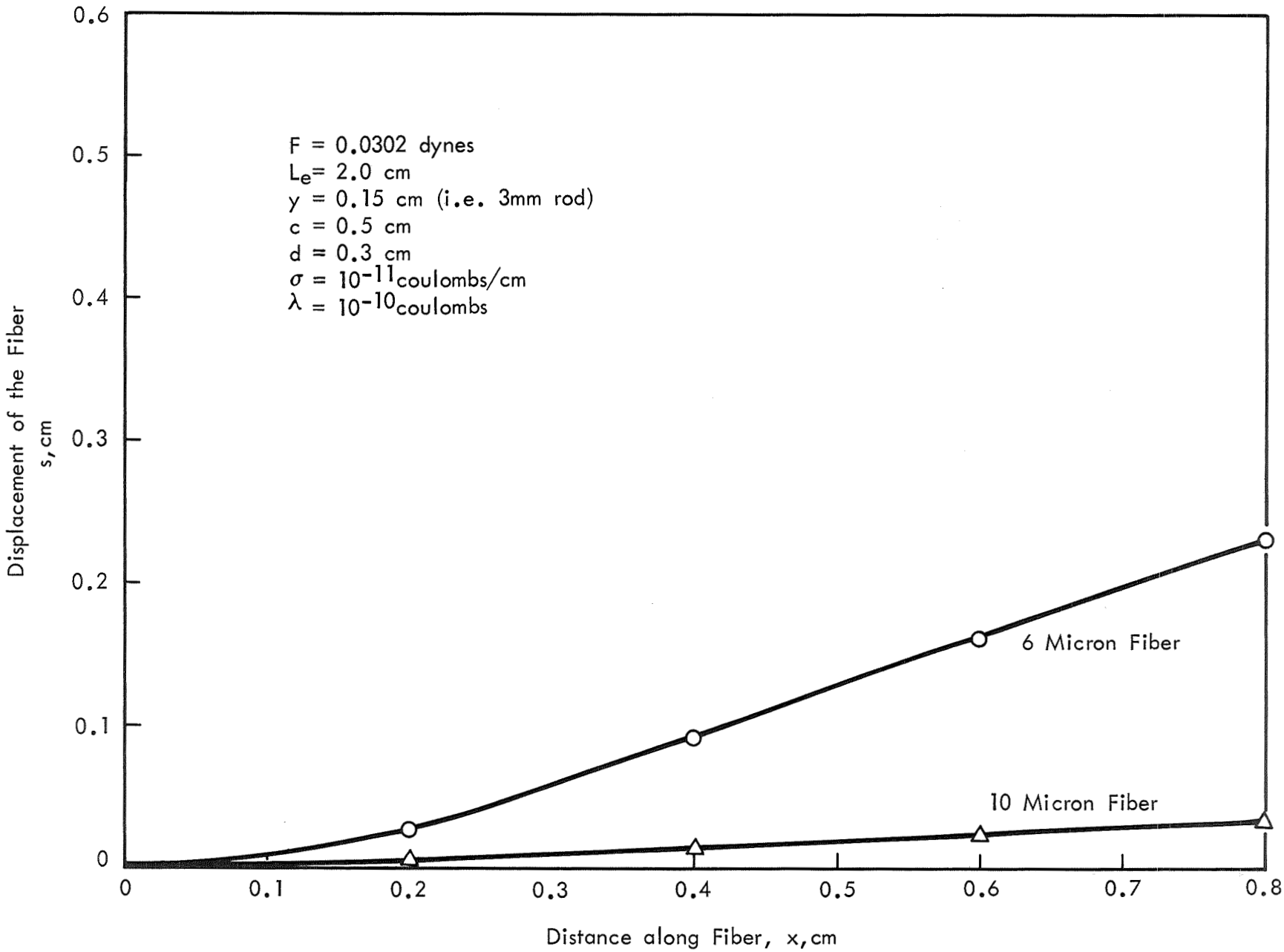


Figure 2-7 Comparison of Fiber Liftoff Distance for Two Fiber Diameters

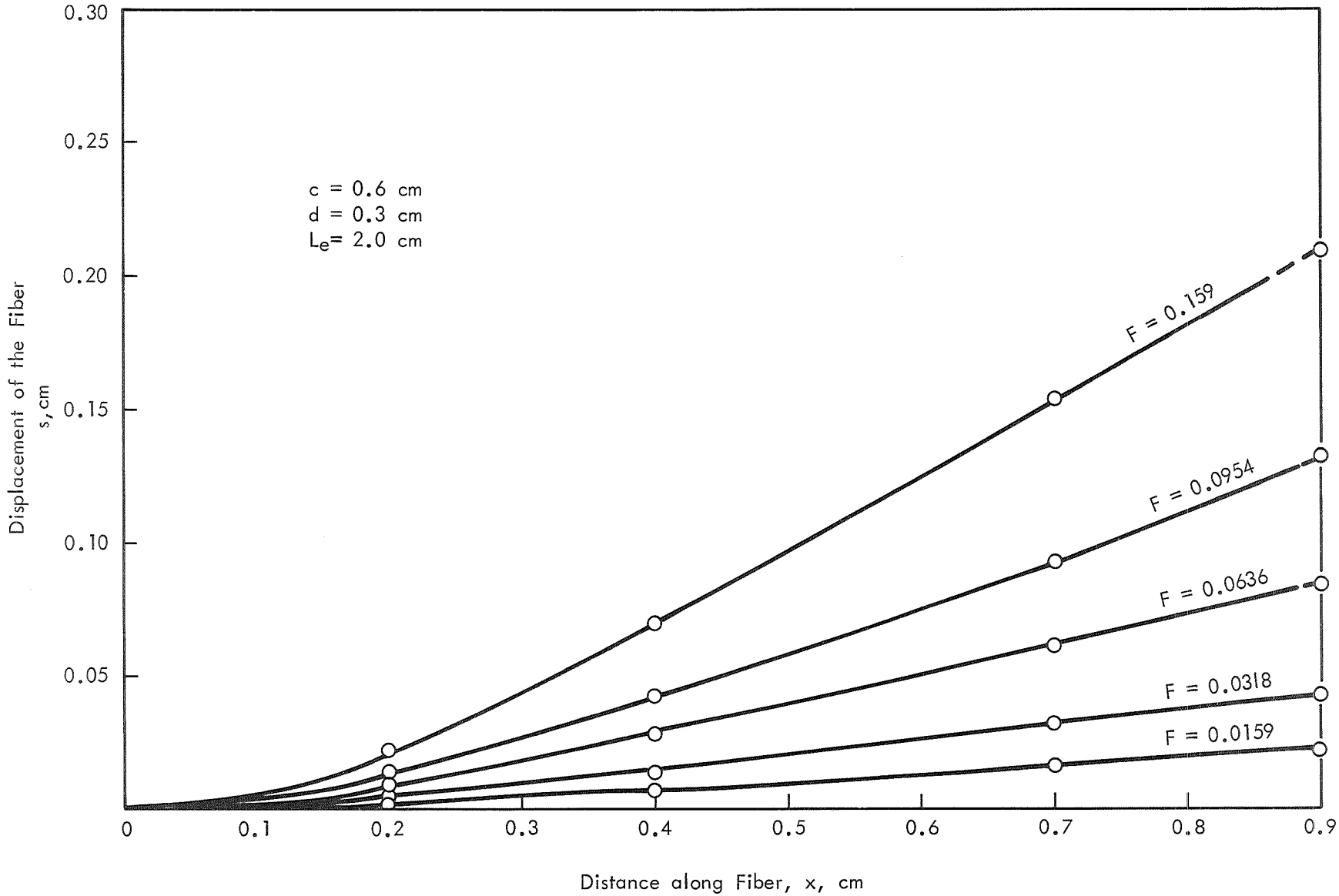


Figure 2-8 Variation in Liftoff Distances of 10 Micron Fibers from 3 mm Rods for Several Values of the Repulsive Force

## 2.2 QFE Dosimeter Recycling and Sensitivity Relationships

The QFE dosimeter operates utilizing the Bragg-Gray principle because of its size, nearness to electronic equilibrium, and the similarity of composition of the medium and the gas. Because it operates by the Bragg-Gray principle, many pertinent relationships may be derived. These relationships are presented after the quantities are defined.

### 2.2.1 Definitions

$E$ = #ev/unit mass of medium absorbed by the medium

$\rho$ = Sm/Sg = mass stopping power ratio of medium to gas

$J$ = #ion pairs/unit mass of gas

$w$ = #ev/ion pair of gas

$D$ = absorbed dose, rads

$m$ = mass of gas, grams

$f$ = collection efficiency

$B$ = #coulombs collected on rod per rad dose

$Q_o$ = total charge on QFE when fully charged, coulombs

$C$ = capacitance of QFE chamber, farads

$Q_R$ = charge on QFE when recycle occurs, coulombs

$V_o$ = battery voltage, volts

$\alpha V_o$ = recycle voltage, volts

$S$ = sensitivity, amps/rad/hr

$P$ = pressure, mm Hg (i.e. Torr)

$V$ = volume of chamber, $cm^3$

R = gas constant, 0.0821 l-atom/mol-deg

T = temperature, °K

n = #moles of gas in chamber

M = molecular weight of gas, grams

2.2.2 Derivations

2.2.2.1 Bragg-Gray

The Bragg-Gray theory says that

$$E = \rho J w. \tag{30}$$

The absorbed dose may then be expressed as

$$D = 1.602\ (10^{-14})\ E = 1.602\ (10^{-14})\ \rho J w \tag{31}$$

after converting ev to ergs and remembering 1 rad = 100 erg/gram.

Equation 31 may be modified to read

$$\frac{Jmf}{D} = 6.25\ (10^{13})\ \frac{mf}{w\rho} \tag{32}$$

which is the number of charges collected on the rod per rad dose.

From Equation 32, one obtains

$$B = 10^{-5}\ \frac{mf}{w\rho}\ . \tag{33}$$

It is obvious that

$$Q_o - Q_R = CV_o\ (1-\alpha)\ . \tag{34}$$

Using Equation 34 in 33, one obtains

$$CV_o\ (1-\alpha) = BD = 10^{-5}\ \frac{mfD}{w\rho} \tag{35}$$

which must be satisfied if the recycling is to be done at a dose of D rads.

The sensitivity may be calculated as

$$S = \frac{B}{3600} = 2.78(10^{-9}) \frac{mf}{w\rho} . \quad (36)$$

2.2.2.2 Ideal Gas Law

The above equations may be modified by use of the ideal gas law, that is,

$$m = nM = 1.602\ (10^{-5}) \frac{PMV}{T} . \quad (37)$$

Using Equation 37, 35 and 36 become

$$CV_o\ (1 - \alpha) = 1.602\ (10^{-10}) \frac{PMVfD}{Tw\rho} \quad (38)$$

and

$$S = 4.454\ (10^{-14}) \frac{PMVf}{Tw\rho} . \quad (39)$$

2.2.2.3 Use of Delrin and Ethylene

The QFE dosimeters developed in this work use Delrin walls and ethylene gas to render them tissue equivalent. That this combination will cause the dosimeters to be tissue equivalent is shown in Appendix A.

The recycling and sensitivity relationships developed above may be further modified due to this specification of the construction materials. The use of ethylene gas allows taking M = 28.05 and w = 26.2. The use of a Delrin medium leads to the value of $\rho$ = 0.904. (see Appendix B.)

When applied to the equations resulting from the Bragg-Gray theory, the specified numbers modify them to be

$$CV_o (1 - \alpha) = 4.22 (10^{-7}) mfD \quad (40)$$

and

$$S = 1.174 (10^{-10}) mf. \quad (41)$$

When applied to the equations resulting from the ideal gas law and the Bragg-Gray theory, the expressions become

$$CV_o (1 - \alpha) = 1.897 (10^{-10}) \frac{PVfD}{T} \quad (42)$$

and

$$S = 5.275 (10^{-14}) \frac{PVf}{T} . \quad (43)$$

2.2.2.4 Graphical Results

The derived relationships for the recycling condition and the sensitivity (i.e. Equations 42 and 43) when the materials are specified and the ideal gas law is used in conjunction with the Bragg-Gray theory are, of course, only approximations. These approximations may, however, be used to predict definite performance trends for the QFE dosimeters. Figures 2-9 and 2-10 demonstrate for visual perusal the inter-relationships between the relevant variables for reasonable values of the variables.

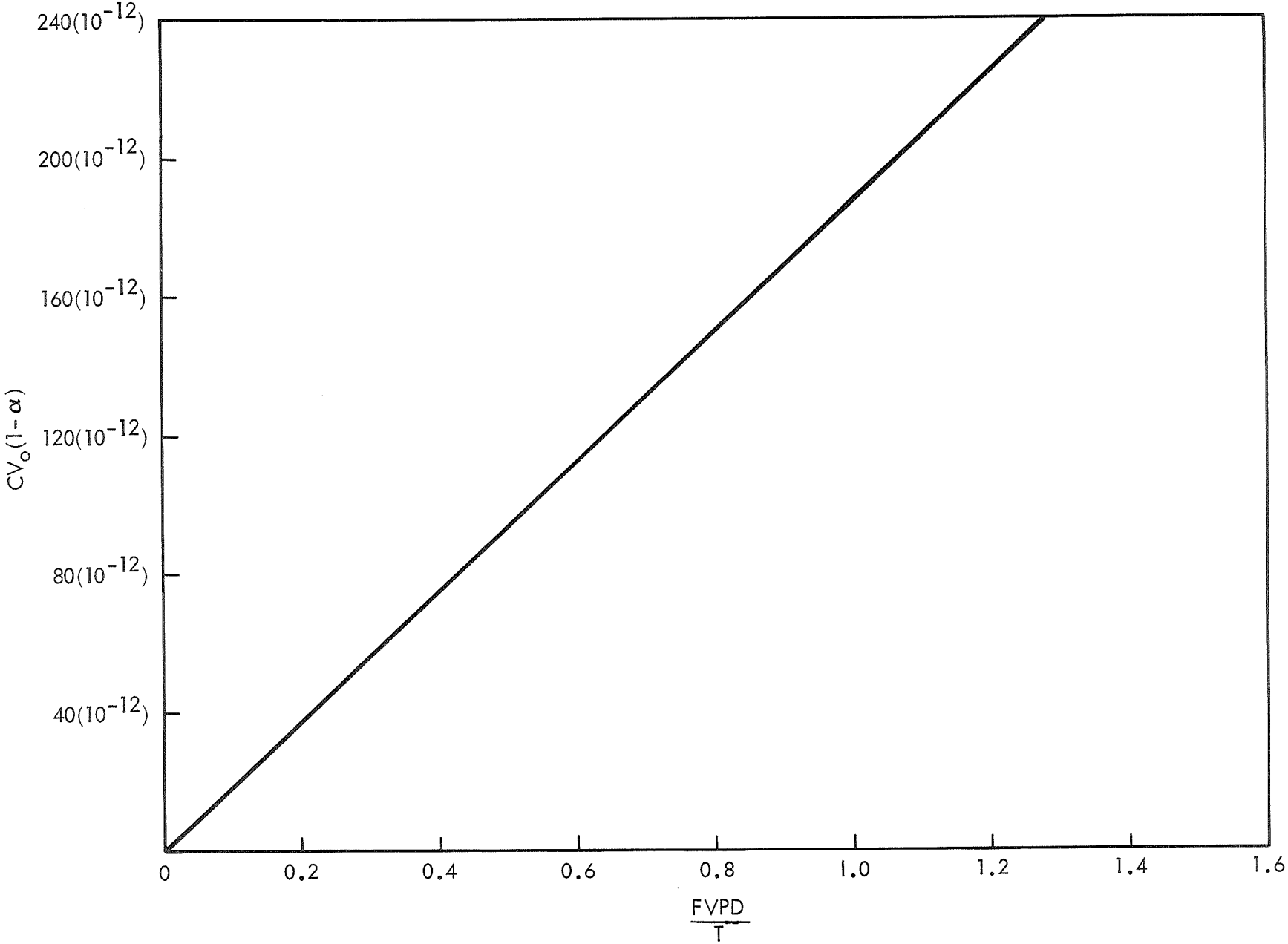


Figure 2-9 Recycling Condition Relationships from Equation 42

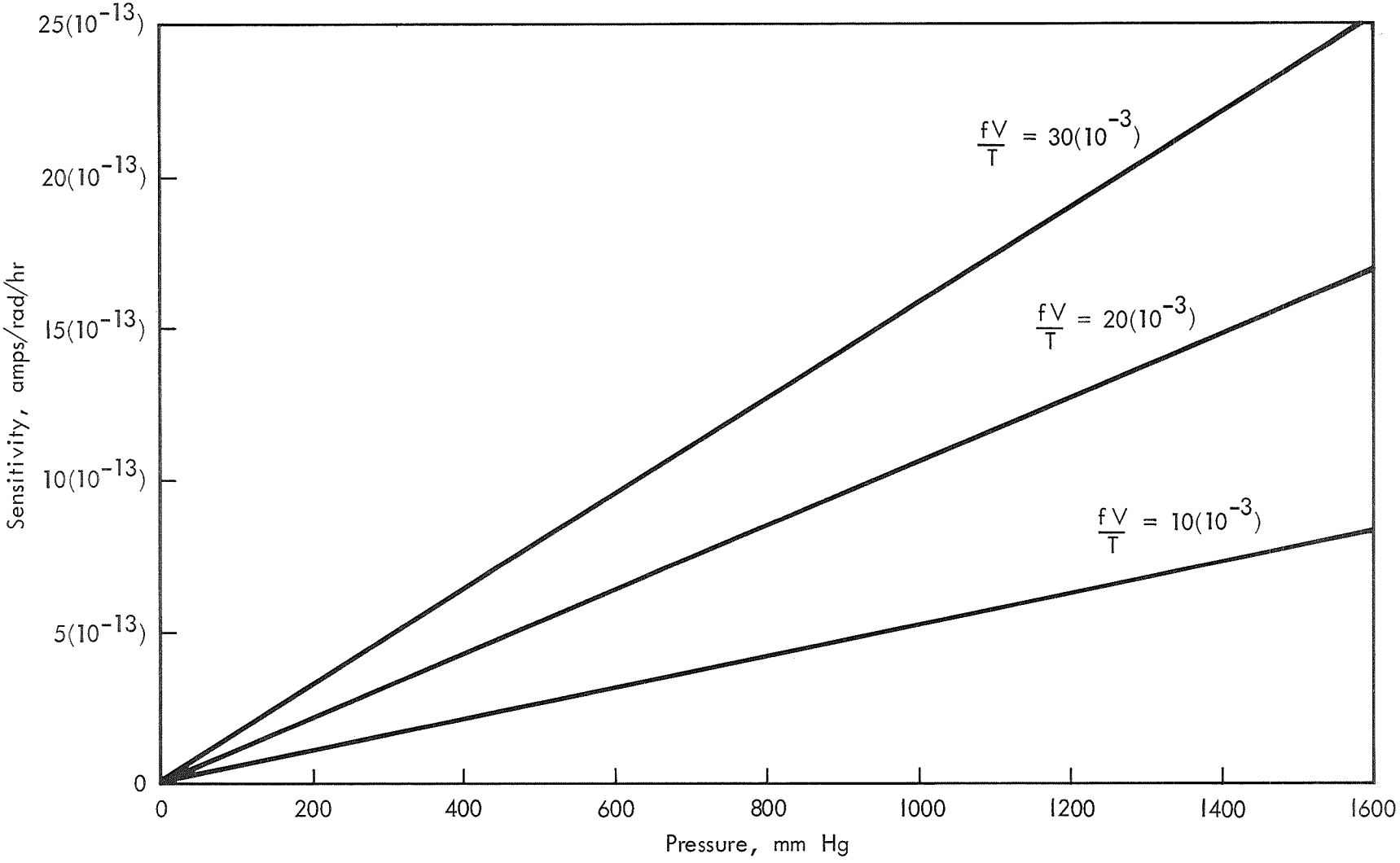


Figure 2-10 Sensitivity Relationships from Equation 43

# III. DESIGN, DEVELOPMENT, AND CONSTRUCTION

The QFE dosimeters were designed, developed, and constructed following the two basic guidelines:

A. The QFE assembly is to be of the type originally described by Neher.[2]

B. The QFE dosimeter is to be small and tissue-equivalent.

## 3.1 The QFE Assembly

### 3.1.1 Development of Essential Capability

The primary difficulty, according to several companies contacted, involved in building the QFE is obtaining uniform quartz fibers of small diameter (i.e. the order of 10 microns). A GDFW technician, after instruction from an experienced quartz-workman*, is able to consistently obtain the desired fibers. The method used to do this is essentially the one described by Neher[12] utilizing the force of the flame to elongate the thin fibers.

### 3.1.2 Evolution of the QFE Assembly

The QFE did not, of course, assume their final designed form until after a substantial amount of experimental work had been done. The purpose of the following discussion is to briefly trace the progress of the QFE to the point where their use inside the TEIC became feasible.

---

*Dave Holcombe, General Electrodynamics Corporation, 4430 Forest Lane, Garland, Texas 75040

3.1.2.1 Description of Assemblies Tested

3.1.2.1.1 Size. The approximate size of the QFE assemblies was determined by the desire to keep the dosimeters small (i.e. ~ 5-15cc). The quartz fiber diameter was fairly early determined to be about 10 microns both from the examination of previous work[2,4] and from the theoretical deflection calculations presented in the preceding Section. The range of sizes investigated is indicated in Table 3-1.

Table 3-1 Range of QFE Sizes Investigated

| Item | Symbol | Size Range | QFE Schematic |
|---|---|---|---|
| | | | |
| Rod Length | a | 24 - 42 mm | 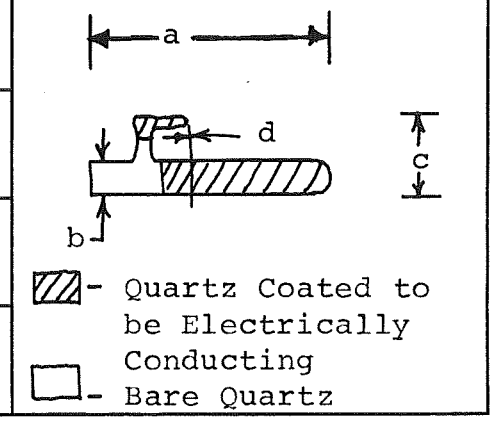 |
| Rod Diameter | b | 2 - 6.35 mm | |
| Fiber Length | c | 7 - 14 mm | |
| Fiber Diameter | d | ~ 5 - 15 microns | |



3.1.2.1.2 Conductive Coatings. Neher[2] utilized Aquadag (i.e. colloidal graphite) to coat the quartz rods and gold to coat the fibers. He also indicated that a gold rod and a gold fiber combination produce cohesive forces so great that the fiber will not always fly away. Neher[4] later produced an instrument that utilized Aquadag for all conductive surfaces.

The conductive coatings tested on the QFE assemblies include all combinations of gold and Signa-Kote*. Signa-Kote is essentially the same as Aquadag, but is more conveniently sprayed and may be purchased ready for use.

The various combinations of conductive coatings tested are shown in Table 3-2 along with their respective resistance readings. The resistance for the NC type units (fiber originally away from rod) is that taken when the fiber makes contact with the rod. The resistance of the entire unit is, however, essentially that of the coated quartz fiber.

Table 3-2 Summary of Conductive Coatings and Resistance Values for All Units Constructed

| Rod/Fiber Coating | Resistance, KΩ | | | Measuring the Resistance |
|---|---|---|---|---|
| | Low | High | Average | |
| Signa-Kote/Gold | 0.034 | 110 | 12.8 | 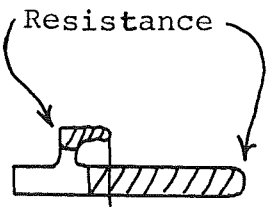  |
| G/G | | | | |
| | | | | |
| S/S | 145 | 12,000 | 1,530 | |
| G/S | | | | |

*Signa-Kote is a product of Mealey Grease and Oil Co., 17509 So. Miles Road, Cleveland, Ohio 44128. It appears to be a finely divided graphite suspended in a chlorinated hydrocarbon such as carbon tetrachloride, trichloroethylene, parachloroethylene, or a mixture of these. Upon evaporation of the carrier, a dry coating is deposited.

3.1.2.1.3 Rod Shape. Traditionally, the coated quartz rods have been cylindrical in shape. The assemblies tested were generally of this traditional cylindrical shape, but several assemblies had a flattened portion along the rod where the fiber made contact. This flattened "side" allows greater forces to be developed because the charges on the rod and on the fibers are nearer one another than in the plain cylindrical shape.

3.1.2.1.4 Photograph of Some Test Assemblies. A photograph of four types of QFE assemblies tested is shown as Figure 3-1. The right hand wire on each assembly is for out-of-chamber testing purposes and is not present when the units are inserted in ionization chambers. It should be noted that these units were among the earliest ones built and are somewhat rough in appearance. A brief description of the units in the photograph is presented in Table 3-3 moving clockwise from the upper right hand assembly.

Table 3-3 Description of QFE in Figure 3-1

| Rod/Fiber Coating | Flat Side? | Resistance, ohms | Rod Length, mm | Rod Diameter, mm | Fiber Length, mm | Fiber Diameter, microns |
|---|---|---|---|---|---|---|
| Gold/Gold | Yes | 1,500 | 24 | 4 | 8 | 10 |
| Signa-Kote/G | No | 6,700 | 28 | 3 | 10 | 10 |
| G/G | No | 1,000 | 25 | 3 | 10 | 10 |
| S/S | Yes | 350,000 | 28 | 4 | 11 | 10 |

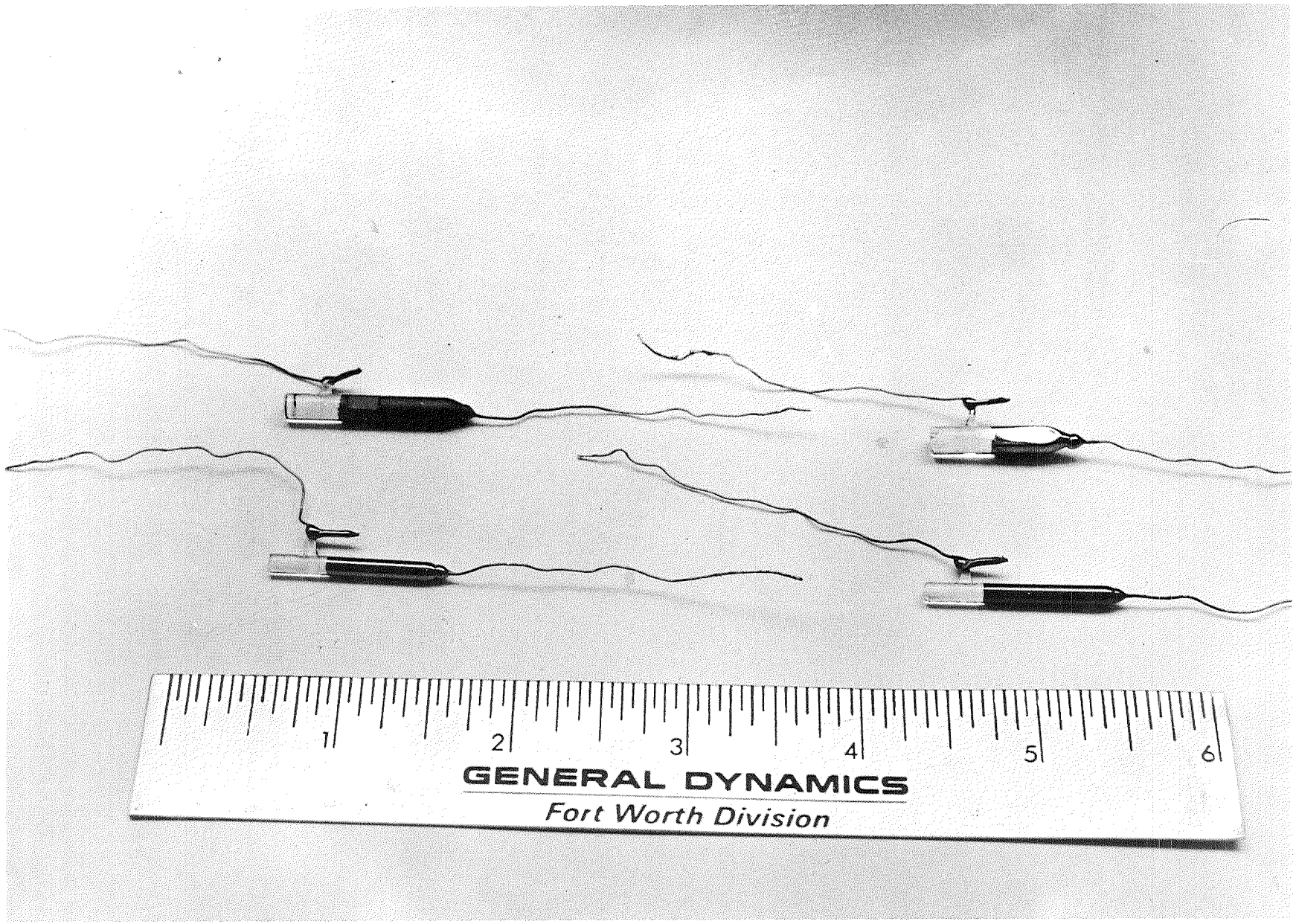


Figure 3-1 Various QFE Test Assemblies

3.1.2.2 QFE Development Tests

The apparatus utilized in the development testing of the QFE is designed to be versatile. It is simple and uncluttered for the gross testing to determine whether or not the units will operate, but is easily modified to examine pulse shapes when required. The reader is requested to remember that this particular discussion is limited to the development of the recycling QFE assembly itself and it is not mounted in the TEIC to form the complete dosimeter.

3.1.2.2.1 Test for Recycling Operation. The schematic for the gross recycling test circuitry is shown in Figure 3-2. This testing was done with a negative voltage on the fiber in order to allow simulation of the radiation. When the 610C is set on $10^n$ ohms, it furnishes a $10^{-n}$ amp current and displays the voltage on its meter. When the QFE operates properly, the following sequence occurs: the voltage is applied to the fiber, the rod and fiber are charged up, the fiber flies away from the rod, the charge on the rod is drained (neutralized) by the 610C current, the fiber returns to the rod, and the cycle is repeated. The voltage at which the fiber flies away as well as that to which the rod falls before the fiber returns may be determined by simply observing the 610C meter.

Figure 3-3 is a photograph of the basic test assembly. Several of the QFE are in the desiccant jar on the clean bench. The Cu sheet attached to the breadboard forms the central portion of the test assembly. The bare quartz portion of the QFE is inserted in a cork

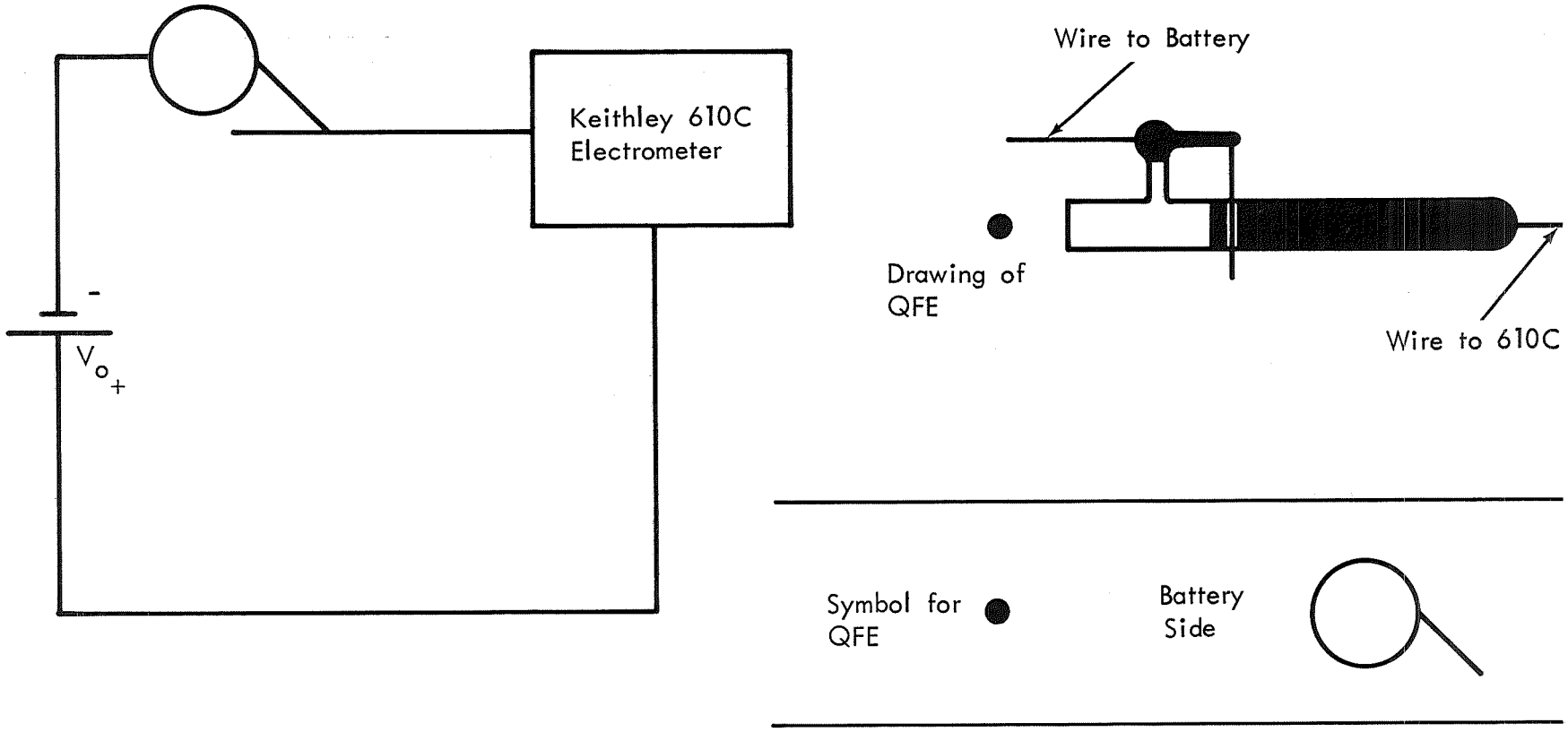


Figure 3-2 Schematic for Gross Recycling Tests

Figure 3-3 QFE Development Test Area

which in turn is held in place by the curved Cu sheet. The alligator clips mounted on the jar lid in front of the 610C proved convenient by holding the QFE by the lead wires while making the experimental arrangements.

3.1.2.2.2 Tests for Pulse Characteristics. The pulse characteristics of the QFE may be determined with the circuit whose schematic is shown in Figure 3-4a. This circuit, in relationship to the Cu sheet/breadboard combination is shown in Figure 3-4b. Results of tests conducted in this manner influenced the design of the amplifier for use with the complete QFE dosimeter. A complete electronics discussion is presented in Chapter 4.

3.1.2.3 The Optimum QFE

The optimum QFE was selected on the basis of the performance of all the units tested in the manner already described. The particular characteristics that were found on the most successful units were incorporated to define the optimum unit. The optimum parameter determination was undertaken after 22 QFE had been made to recycle. These parameters were determined by examination of the data presented in Table 3-4. A sketch of the optimum QFE with the pertinent parameters shown is presented as Figure 3-5.

After determining the optimum characteristics, the QFE were all constructed with those characteristics in the manner described in the following discussion.

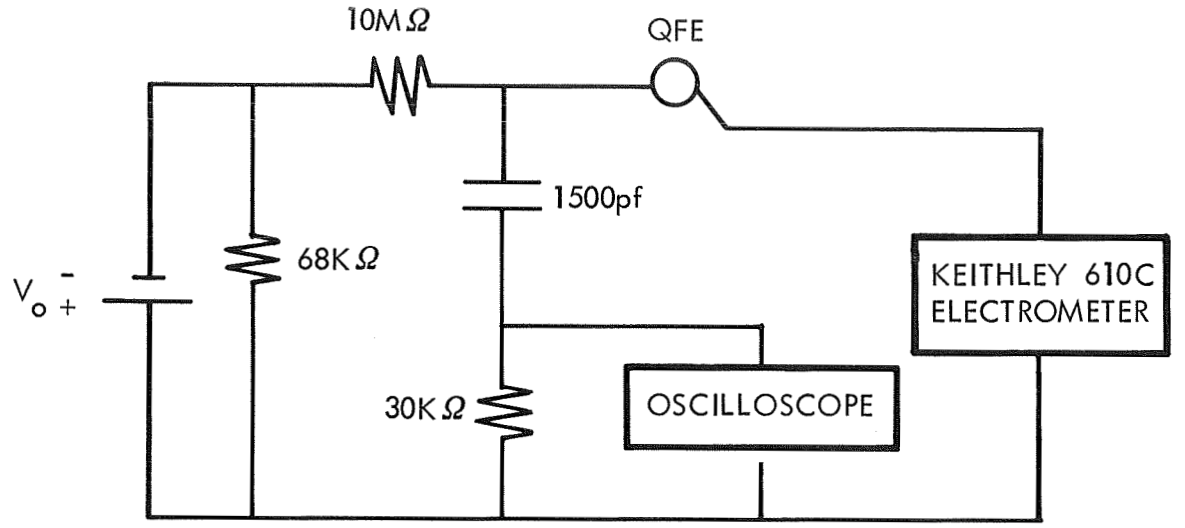


(a) Schematic

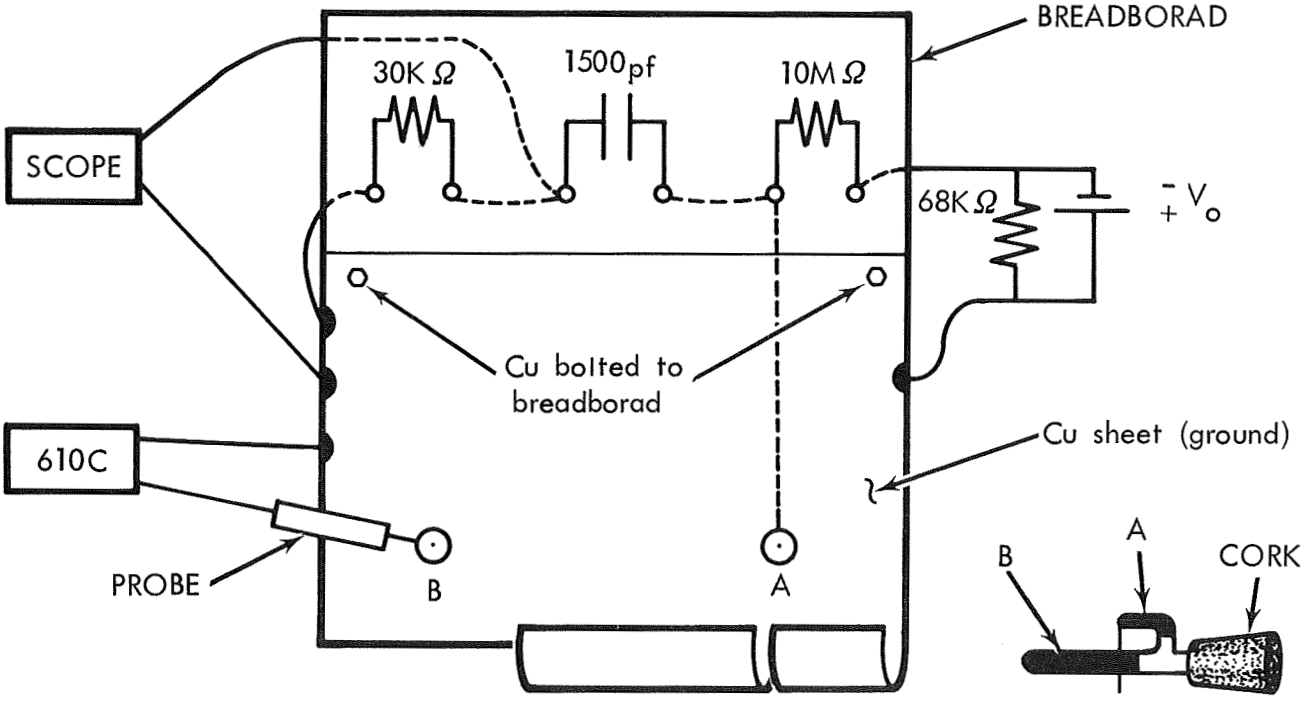


(b) Schematic with Mounting Details

QFE Unit in Cork
Sits in Cu Sheet

Figure 3-4 Circuitry for QFE Pulse Characteristic Test

Table 3-4 Data for Optimum Parameter Determination

1. Rod/Fiber Coating

| Variable | # Units with that property | # Tests of that property | # Recycle tests | % of tests that recycled |
|---|---|---|---|---|
| S/G[1] | 2 | 36 | 7 | 19.4 |
| S/S | 4 | 25 | 8 | 32.0 |
| G/G | 6 | 132 | 37 | 28.0 |
| G/S | 10 | 47 | 29 | 61.7[2] |
| Totals | 22 | 240 | 81 | 33.8 |

2. Rod Diameter (mm)

| | | | | |
|---|---|---|---|---|
| 2 | 1 | 23 | 1 | 4.3 |
| 3 | 7 | 55 | 28 | 50.9[2] |
| 4 | 6 | 104 | 26 | 25.0 |
| 6.35 | 8 | 58 | 26 | 44.8 |
| Totals | 22 | 240 | 81 | 33.8 |

3. Rod Length (mm)

| | | | | |
|---|---|---|---|---|
| 24-26 | 4 | 94 | 24 | 25.5 |
| 28 | 4 | 33 | 10 | 30.3 |
| 30 | 10 | 47 | 32 | 68.1[2] |
| 32-42 | 4 | 66 | 15 | 22.7 |
| Totals | 22 | 240 | 81 | 33.8 |

4. Flat Side (yes or no)

| | | | | |
|---|---|---|---|---|
| Yes | 12 | 118 | 55 | 46.6[2] |
| No | 10 | 122 | 26 | 21.3 |
| Totals | 22 | 240 | 81 | 33.8 |

5. Resistance (megohms) - units with gold rod, Signa-Koted fiber

| | | | | |
|---|---|---|---|---|
| <.145 | 0 | 0 | 0 | 0 |
| .145-.24 | 1 | 5 | 1 | 20 |
| .25-1.5 | 7 | 35 | 21 | 60[2,3] |
| 1.51-2.7 | 1 | 3 | 3 | 100 |
| > 2.7 | 0 | 0 | 0 | 0 |

1 S denotes Signa-Kote, G denotes gold.
2 Denotes % defining the optimum variable.
3 The performance of the units in recycling, independent of the percentage of recycle tests, was best in this range.

- Rod Coating - Gold
- Fiber Coating - Signa-Kote
- Rod Length - 30 mm
- Rod Diameter - 3 mm
- Rod Peculiarities - Partially flattened side for better fiber contact
- Resistance - 0.25 - 1.5 Megohoms (Measured A to B)


- Uncoated Quartz


- Gold Coated Quartz

QFE SKETCH IS DOUBLE ACTUAL SIZE

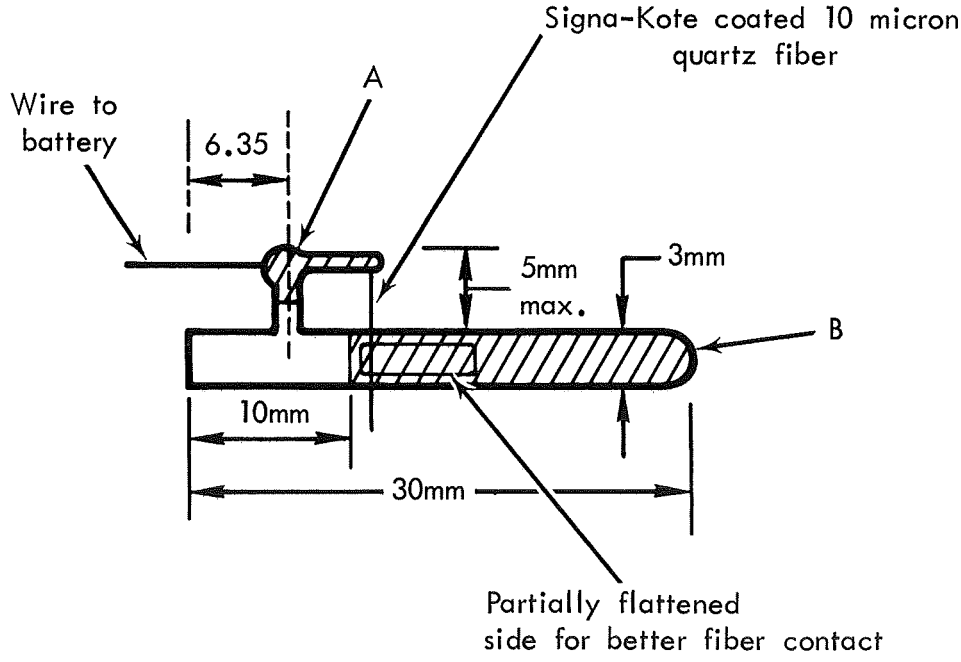


Figure 3-5 The Optimum QFE Parameters

### 3.1.2.4 Construction Procedure

Many procedures were attempted before settling on the ones used for construction of the QFE with optimum parameters. Cleanliness is very important to the success of the QFE and the materials from which the units are made are carefully cleaned and handled. The assembly work is done on a clean bench and the units not in use are stored in a clean, dry environmental jar.

The thin gold coating of the quartz rod is accomplished using the equipment shown in Figure 3-6. Approximately 1 gram of gold is placed in a tungsten boat between the electrodes. The QFE are attached by their lead wires to the gears above the electrodes. The system is evacuated to about $10^{-5}$ Torr, the gears are rotated so as to allow uniform coating of the units, and current is applied to the boat through the electrodes to evaporate the gold onto the QFE.

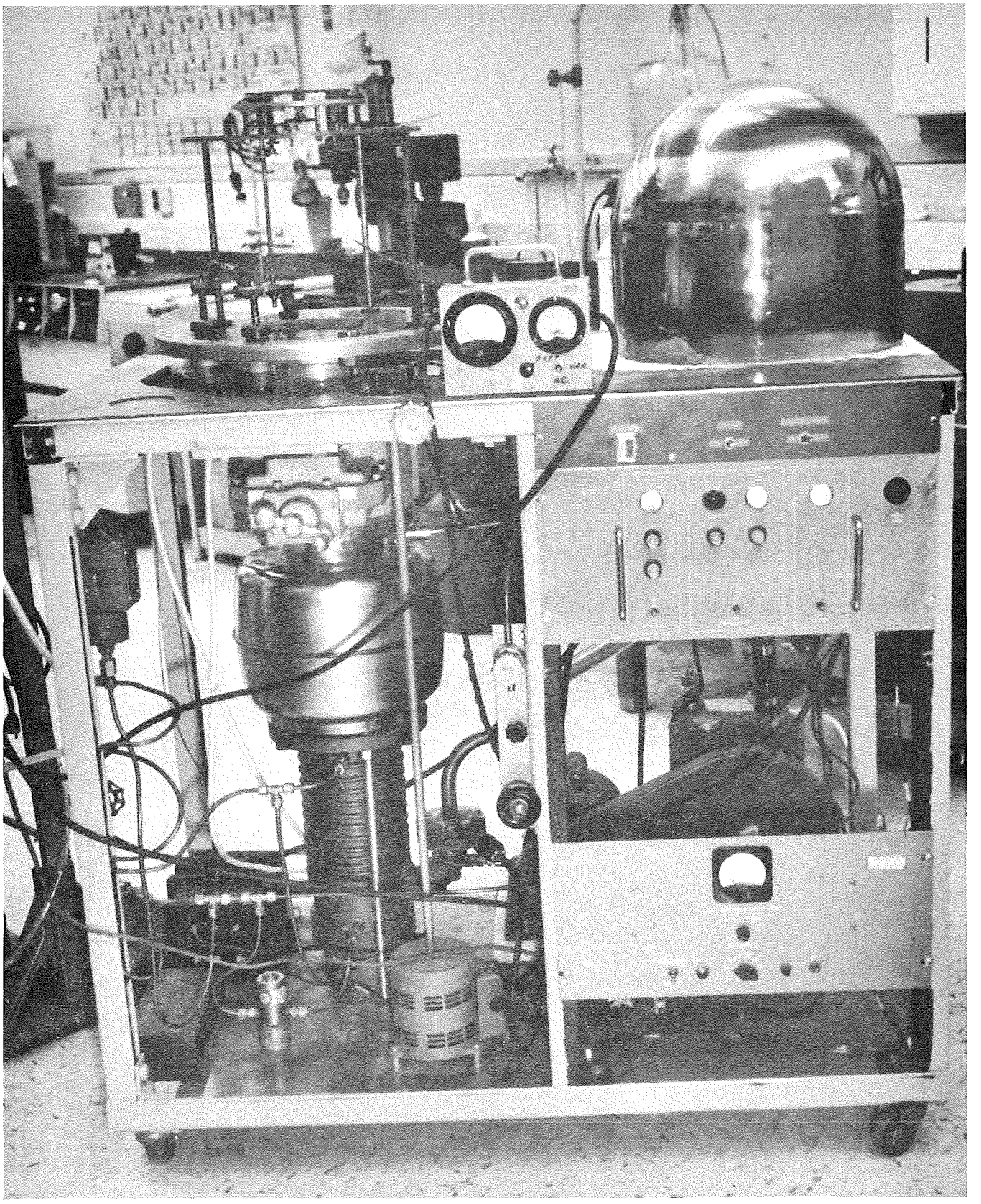

Figure 3-6 Equipment for Gold Coating the Quartz

The quartz fibers are spray coated with Signa-Kote while spinning rapidly in a lathe. It is hoped that the spinning action will allow a fairly uniform coating to be obtained. The coating is continued until resistances in the neighborhood of 0.25 - 1.5 M$\Omega$/cm are obtained.

The complete procedure for the construction and care of the assemblies is outlined and presented as Figure 3-7.

## 3.2 The TEIC

The basic idea behind the construction of a tissue equivalent ionization chamber (TEIC) is to measure the so-called "tissue-rad," that is, 100 ergs/gram absorbed in human muscle tissue. The chamber materials and design must be carefully selected in order to meet this requirement.

### 3.2.1 Materials Selection

The ionization chamber designed to house the QFE assembly is tissue equivalent by virtue of having Delrin walls and being filled with ethylene gas (1 atm. pressure is used to minimize leakage problems). It is shown in Appendix A that this combination does indeed allow the construction of the TEIC.

The materials other than Delrin and ethylene used in the QFE dosimeter are quartz and aluminum. The quartz forms the detection element while the aluminum forms the cover and backplate of the completed unit. The 6061 aluminum was selected because of already being NASA approved as well as being readily available. Physical properties of quartz and aluminum as well as those of Delrin and

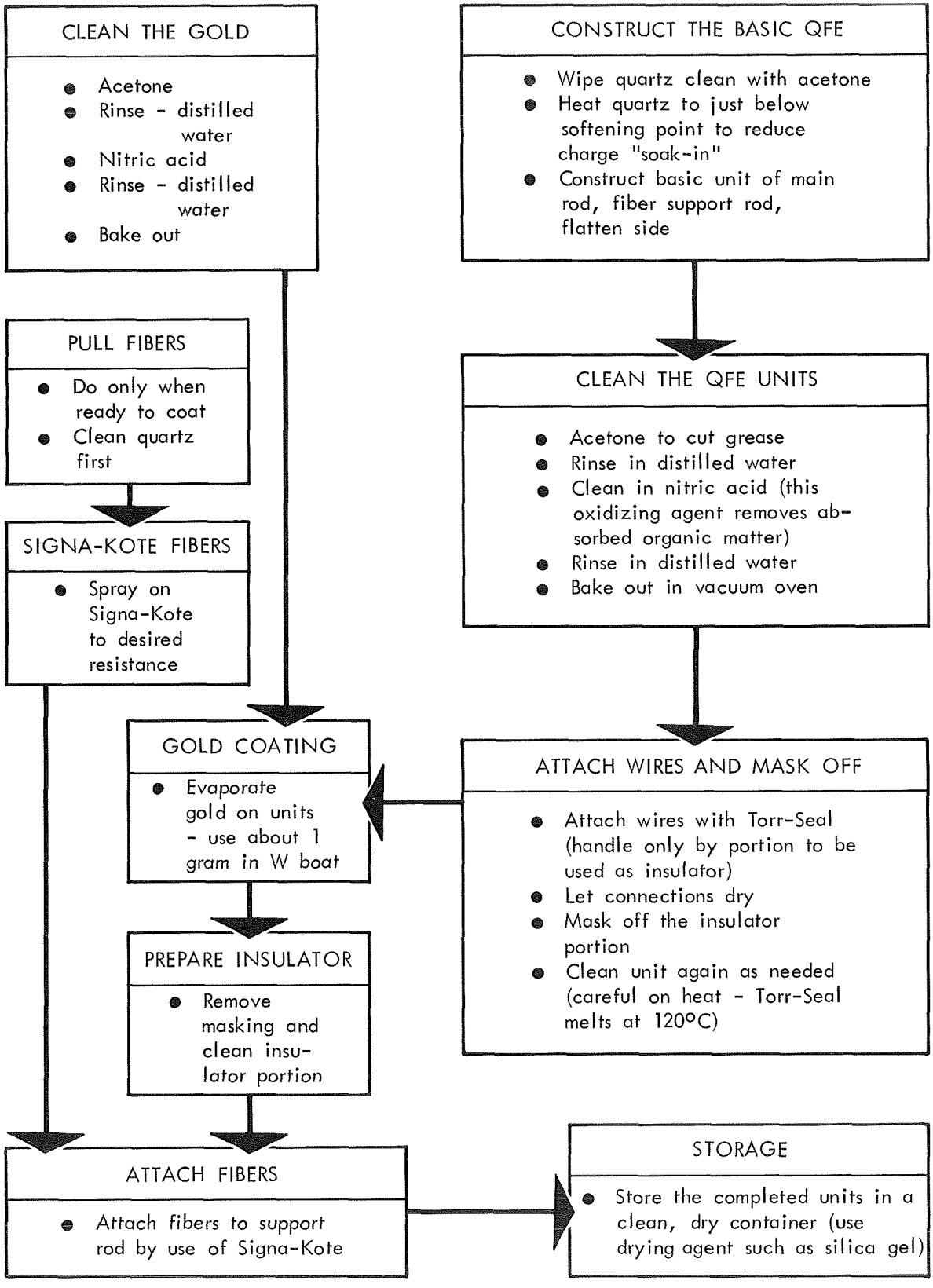


Figure 3-7 QFE Construction Procedure

ethylene are presented in Appendix C.

### 3.2.2 Chamber Characteristics

The chamber characteristics are shown in Table 3-5 and briefly discussed below.

The chamber size is approximately determined by the size of the QFE assembly. The chamber must provide adequate clearance for the QFE at the end as well as all around.

The thickness of the wall formed by the Al cover and the Delrin electrode is determined by the requirement that the electrons reaching the gas volume be essentially those "knocked out" of the Delrin when the dosimeter is subjected to a gamma field.

## 3.3 The Complete QFE Dosimeter

The complete QFE dosimeter assembly which, without the gas fill tube, weighs approximately 23 grams is shown in Figure 3-8. The exploded view of the dosimeter includes the following items from right to left: Al cover, Delrin electrode partially coated with Signa-Kote and the Cu piece to assure good contact with the Al, QFE, Delrin support, signal contact, indium seal, chamber backplate with feedthrough and gas fill tube, and chamber screws.

Table 3-5

Chamber Characteristics

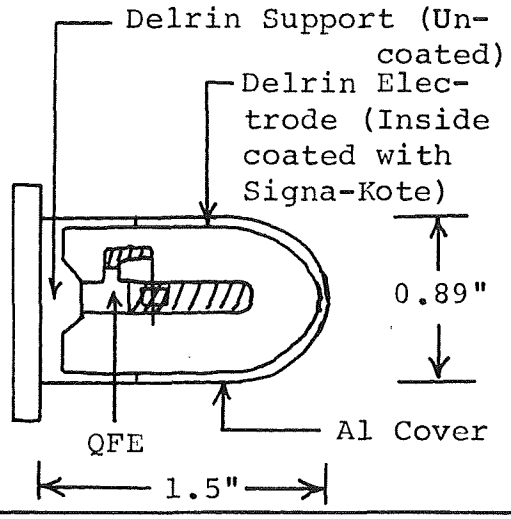


Signa-Kote Coated Delrin Electrode

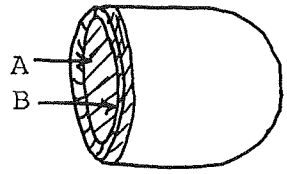


$R_{AB} < 20{,}000$ ohms

The volume of the chamber (less the volume of the QFE and the Delrin) is about 9cc($0.55 in.^3$)

| Material | Wall Thickness, cm | Wall Thickness, mils | Wall Thickness, $g/cm^2$ |
|---|---|---|---|
| Al | 0.0381 | 15.0 | 0.103 |
| Delrin | 0.0800 | 31.5 | 0.112 |
| Totals | 0.1181 | 46.5 | 0.215 |

| Particle | Symbol | Minimum Energy Particle to Completely Penetrate Al and Delrin |
|---|---|---|
| Beta | $\beta$ | ~ 0.62 Mev |
| Proton | p | ~ 11.6 Mev |
| Alpha | $\alpha$ | ~ 46.4 Mev |

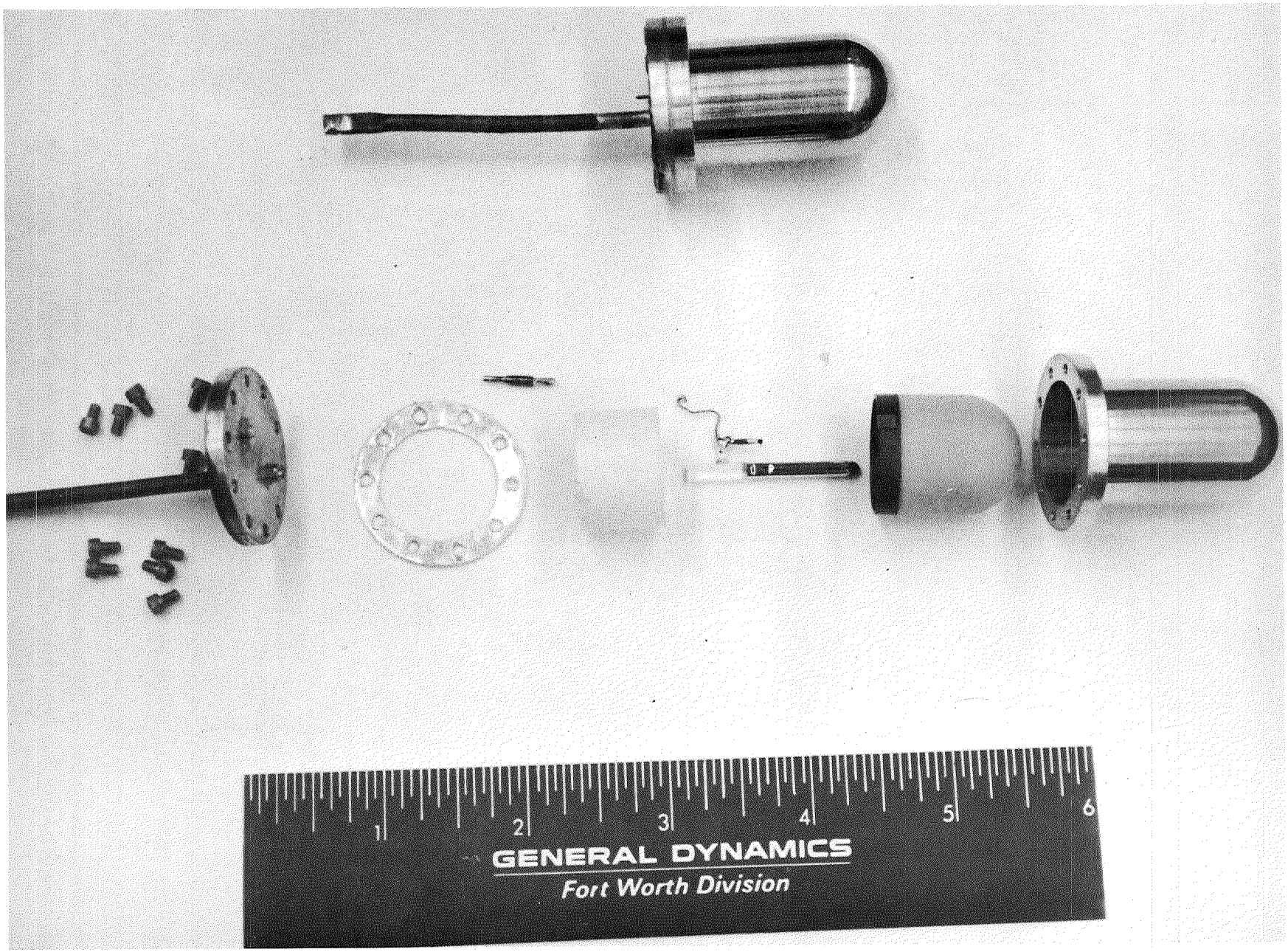


Figure 3-8 Quartz Fiber Electrometer Dosimeter

# IV. ELECTRONICS

The purpose of this discussion is to show how the experimental data was taken and to describe the relevant circuitry and electronic components. The output of a further developed QFE dosimeter would probabily be on a visual digital display (e.g. electroluminescent) updated by the successive pulses from the dosimeter and with each pulse signifying that a predetermined dose had been absorbed. The present assembly furnishes the same type pulses observed in various radiation fields. Knowing the time between pulses and the dose rate allows one to calculate the dose absorbed corresponding to a pulse. The instrument may thus be calibrated and be a useful radiation dosimeter. The electronics described below allow the necessary data to be taken.

## 4.1 The Complete Electronics System

The operation of the complete electronics system used in the acquisition of the data is explained with reference to Figure 4-1. The QFE is charged via the Keithley power supply and the fiber is repelled from the rod. As the radiation leads to the ionization of the ethylene gas and as the ions are collected, the charge on the rod is neutralized thus allowing the fiber to again approach the rod. When the charge on the rod becomes so small that the Coulomb force can no longer keep the fiber away, the fiber makes contact with the rod and a pulse is developed as the QFE is re-charged. This pulse is amplified and used to turn on the Canberra

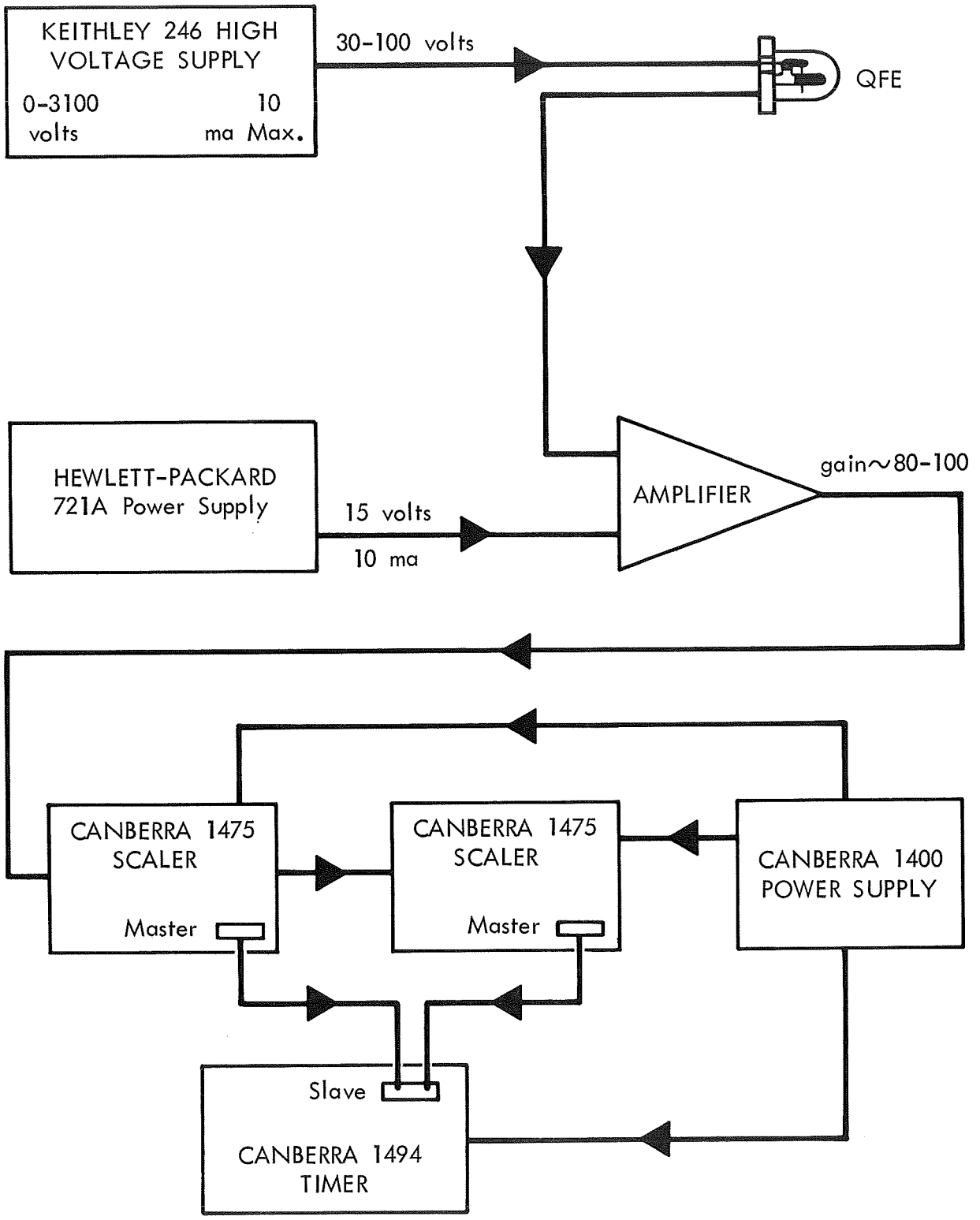


Figure 4-1 Schematic of the Complete Electronics System

timer. The next pulse, or any succeeding one, may be used to turn off the timer. The time for any number of pulses to occur may thus be obtained. Knowing the dose rate from the radiation source allows the calculation of the absorbed dose necessary to cause a pulse and, consequently, the calibration of the QFE dosimeter.

4.1.1 QFE Dosimeter Details

The QFE dosimeter has an extremely small capacitance. The results of measurements made from the feedthrough pin to the chamber backplate with a Tektronix Type 130 L-C meter are presented in Table 4-1.

Table 4-1 Capacitance Measurements

| Unit | Capacitance, pf | |
|---|---|---|
| 3 | 2.0 | |
| 5 | 2.3 | Average = 2.3pf |
| 6* | 2.2 | |
| 8 | 2.7 | |

The charge transfer per pulse is calculated to be approximately $3.5(10^{-11})$ coulombs when 15 volts is taken to be a typical value of the potential difference between the fiber and the rod just prior to recycling. It is recognized that the above figure is very rough (and probably high) since the capacitance of the backplate, feedthrough, etc. are included with that of the QFE chamber in the measured values.

*Denotes NC-type unit described in Section II

### 4.1.2 Amplifier Details

The pulse available for amplification is very dependent on the output capacitance of the dosimeter unit. Referring to Figure 4-2, this capacitance is seen to essentially be the series combination of the two 1500 pf capacitators, that is, 750 pf. The input voltage to the amplifier is then calculated to be approximately 50 mv if the values from 4.1.1 are used.

The response of the amplifier itself was tested using an Intercontinental Instrument Model PG-2 pulse generator and a Tektronix oscilloscope. All the testing was done with +15 volts applied to the amplifier circuit, an input signal frequency of 10 Hz, and a pulse width of 20 $\mu$sec. The results of the tests are shown graphically in Figure 4-3.

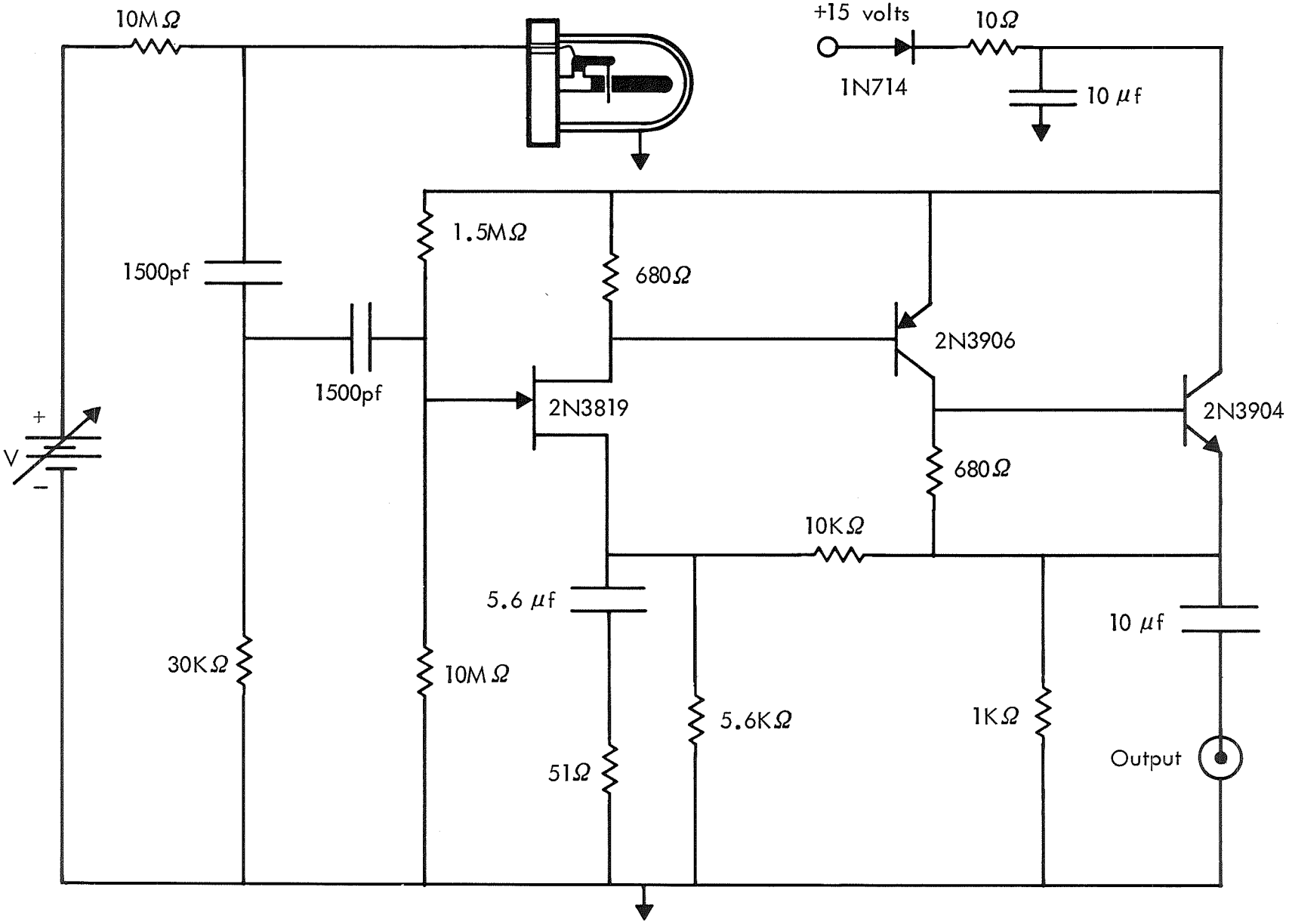


Figure 4-2 Electronics Detail of the QFE Dosimeter and Amplifier

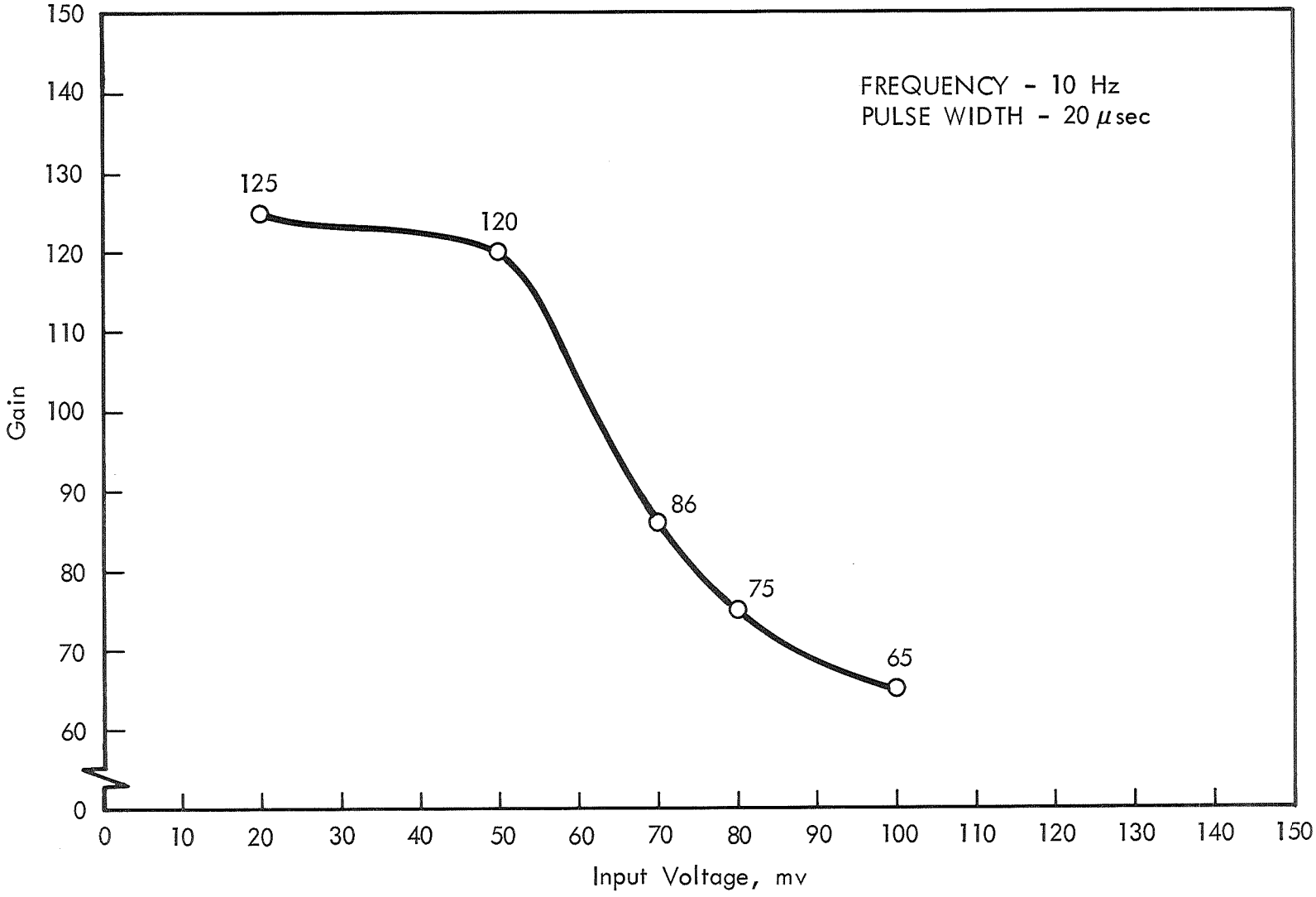


Figure 4-3 Response of Amplifier Used with QFE Dosimeter

# V. DOSIMETER CHARACTERISTICS

The results of the testing of eight QFE dosimeter systems are presented in this Section in both graphical and tabular form. The dosimeters, each filled with ethylene to a pressure of 760 Torr, are numbered from 1 to 8 and are of the "regular" type unless the number is followed by an asterisk which denotes the dosimeter as being of the NC-type discussed in Section II.

## 5.1 Saturation Voltage

Saturation curves were obtained for the dosimeters using the G-367 $^{137}Cs$ source. This source, along with the others used in the experimental work, is described in Appendix D. Saturation data was taken in order to determine the voltage at which to operate the individual dosimeters. The saturation curves are shown in Figures 5-1 and 5-2. The operating voltages determined from these curves are listed in Table 5-1.

Table 5-1 Dosimeter Operating Voltage

| Unit Number | 1 | 2 | 3 | 4 | 5 | 6* | 7* | 8 |
|---|---|---|---|---|---|---|---|---|
| Operating Voltage | 50 | 80 | 30 | 50 | 60 | 30 | 100 | 50 |

## 5.2 Orientation

The saturation curves were determined with the dosimeter fibers approximately in the vertical position and being neither aided nor hindered by the earth's gravitational field. Even though advanced

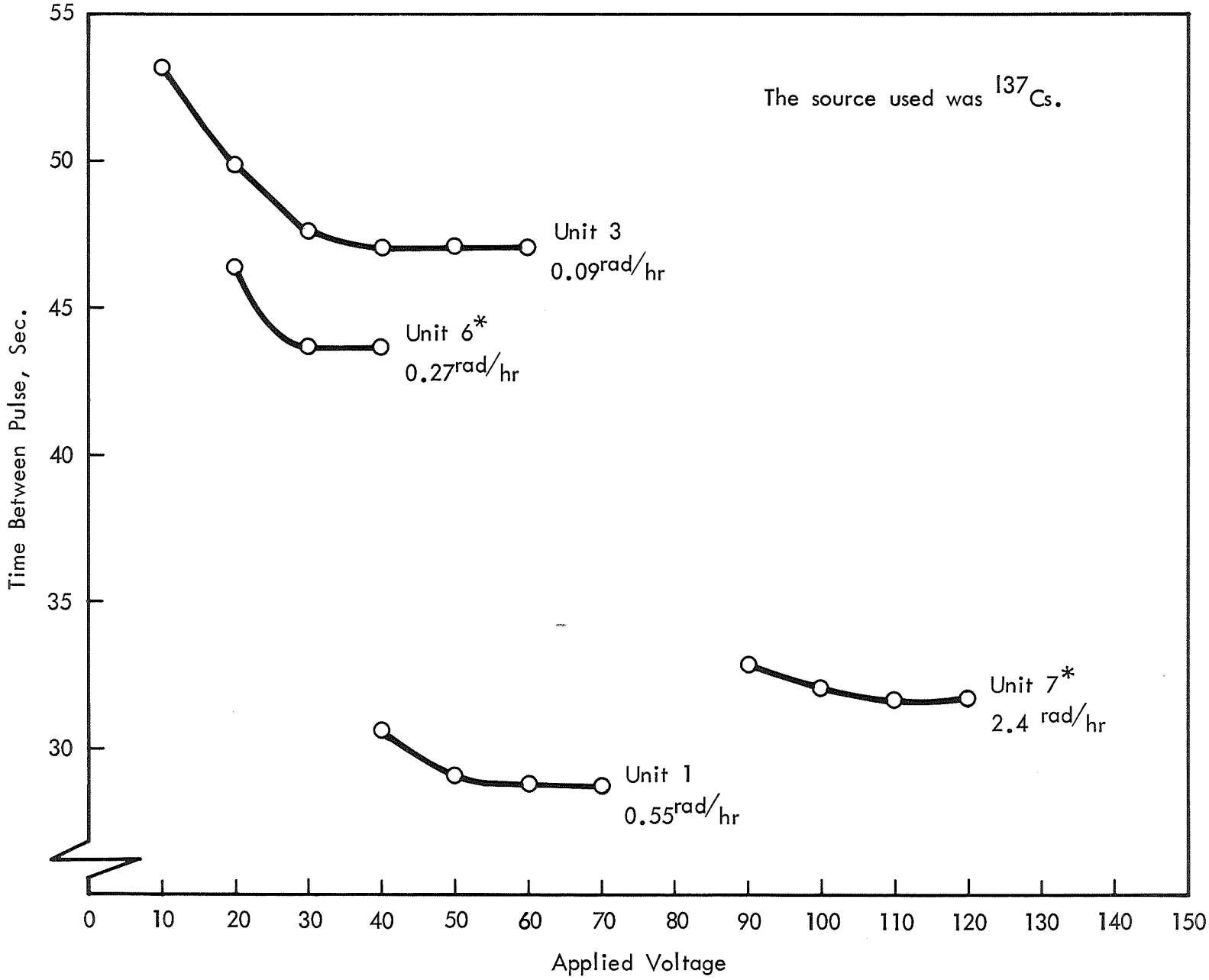


Figure 5-I Saturation Curves for Dosimeters 1, 3, 6,* and 7*

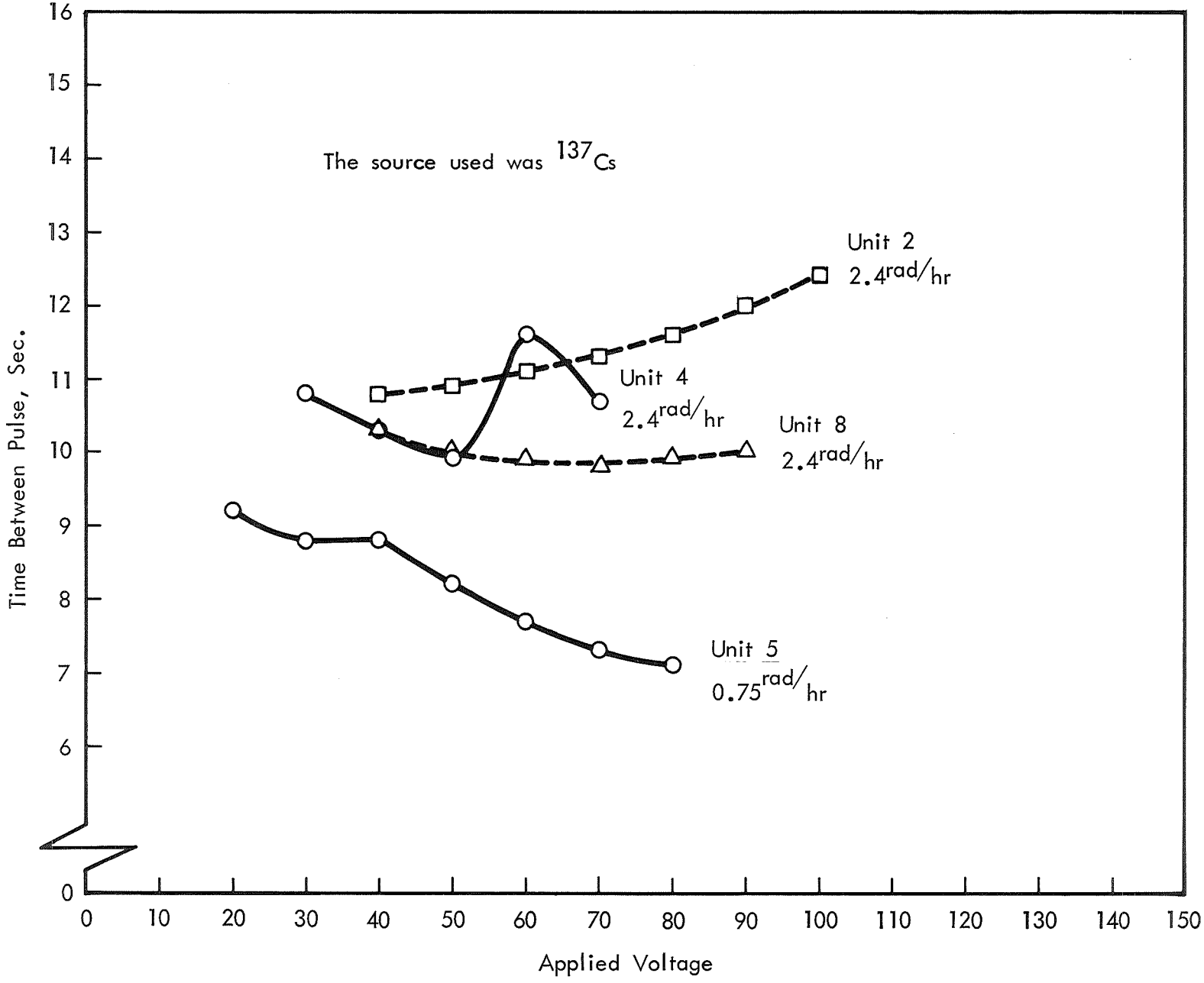


Figure 5-2 Saturation Curves for Dosimeters 2, 4, 5, and 8

dosimeter units of the QFE type may operate in a low (or zero) gravity area, the gravity effect deserves investigation. Orientation tests were performed on the units in the four basic positions described in Figure 5-3. Position 1 is the orientation used in all tests besides these to determine gravity effects.

The orientation tests were performed using the G-367 $^{137}Cs$ source. The test results, considering the time between pulses at position 1 to be taken as 0 deviation, are plotted in Figures 5-4 and 5-5. The results are not symmetrical because the fiber makes an angle of approximately 10° with the vertical or horizontal in each of the test positions (see Figure 5-3). If the fiber positions were truly vertical and horizontal, the deviation for position 3 would have been nearly zero and those for positions 2 and 4 would have had about the same values but opposite signs.

The results vary from unit to unit because of the differences in the tension in the fiber, fiber length, and coating thickness. Dosimeters 3 and 6* are extremely dependent on the orientation, in fact, unit 3 will not operate in position 2. It is of interest to note that the behavior of the NC units (denoted by asterisks) did not significantly differ from that of the "regular" units.

## 5.3 $^{60}Co$ Calibration

The QFE dosimeter systems were calibrated for $^{60}Co$ dose rates varying by approximately five orders of magnitude. Being constrained by the irradiation facilities, the source for rates of 260 mrad/hr

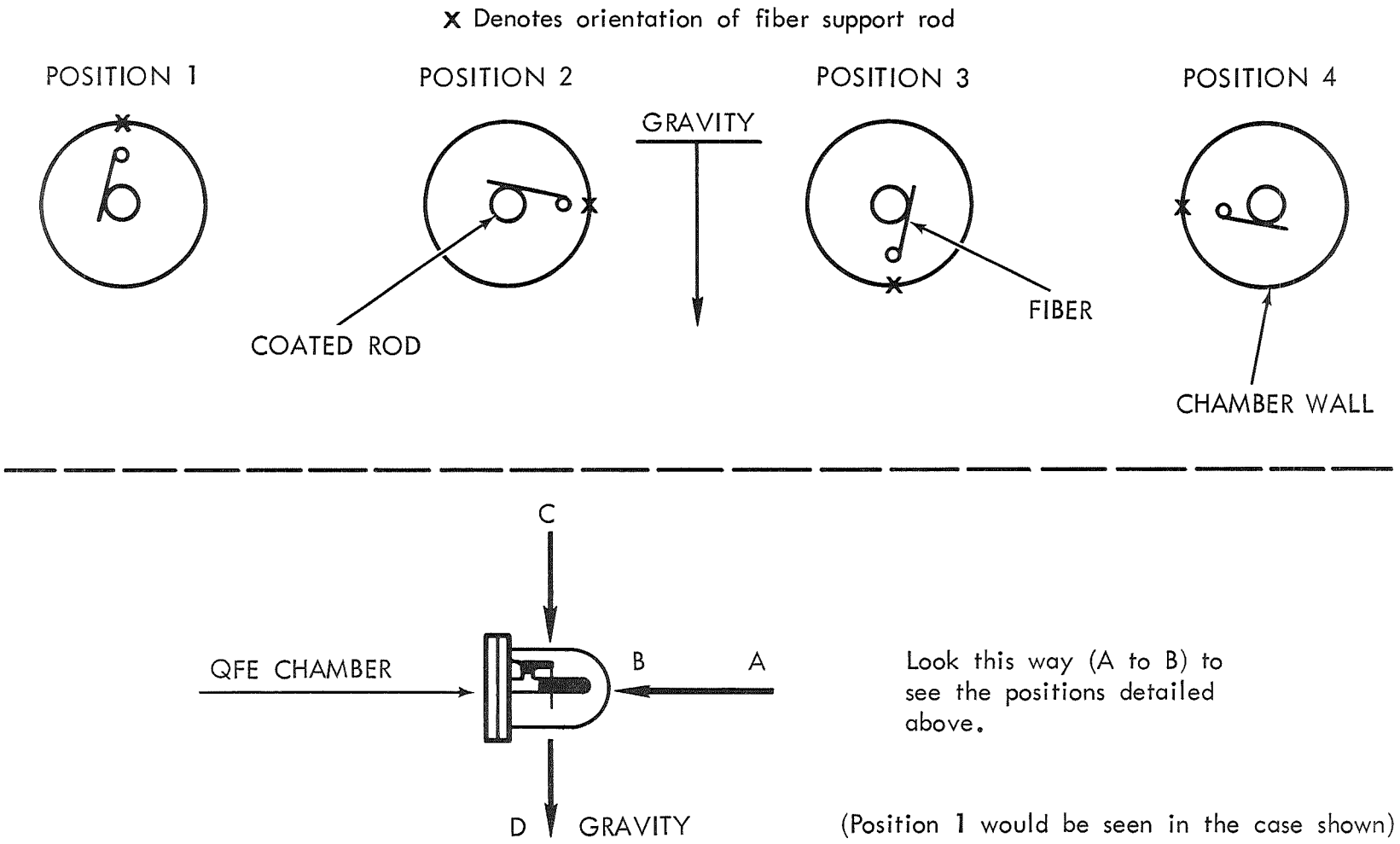


Figure 5-3 Orientation Test Positions

SAMPLE CALCULATION (Dosimeter 2)

| Position | 1 | 2 | 3 | 4 |
|---|---|---|---|---|
| Average time between pulses, sec | 11.6 | 10.3 | 11.9 | 12.8 |

For Position 2, % Deviation = $\frac{10.3-11.6}{11.6} \times 100 = -11.2$

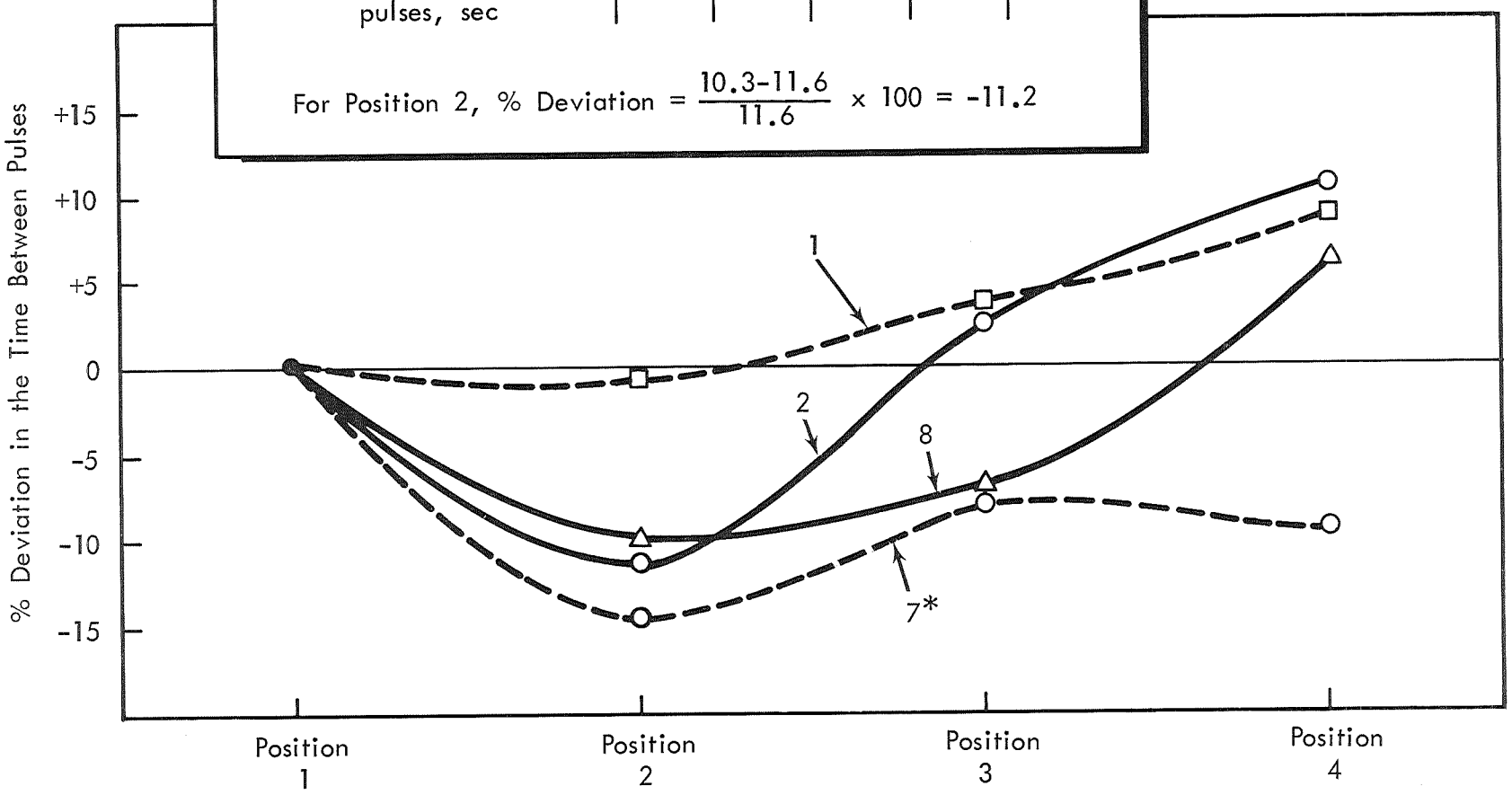


Figure 5-4 Orientation Test Results for Dosimeters 1, 2, 7,* and 8

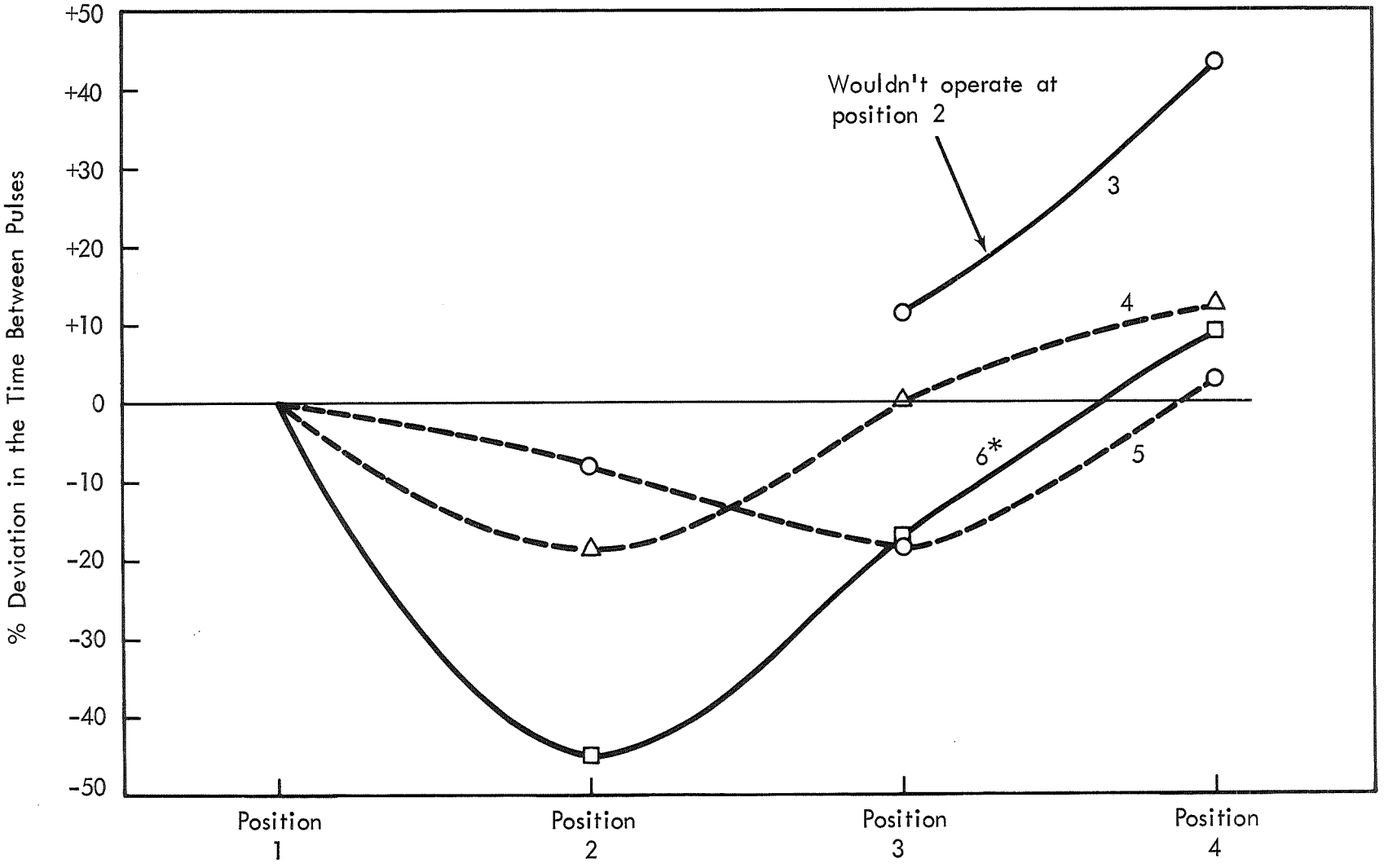


Figure 5-5 Orientation Test Results for Dosimeters 3, 4, 5, and 6*

and above was located below the dosimeters along the line CD in Figure 5-3. The lower dose rate data was taken with the source located along the line AB in the same figure. The calibration data was taken using the experimental configuration described in Section IV and is presented in tabular form in Tables 5-2 and 5-3 while the graphed results are shown in Figure 5-6 and 5-7.

The time between pulses at the lower dose rates is shorter than expected. This results in the absorbed dose per pulse being lower than expected. Charge leakage is rejected as the probable cause of the data being like it is because of the superb insulator properties of quartz. A reasonable explanation is that the background radiation in the Irradiated Materials Laboratory is significant with respect to the very low dose rates. This would cause the observed effect and would be negligible at the higher rates. Little significance is thus attached to the observed relatively low dose per pulse readings at the low dose rates.

While examining the $^{60}Co$ calibration data shown in Figures 5-6 and 5-7, it should be kept in mind that the data covers five decades. The results are quite good for these early developmental units and are nearly linear over a very large range of values. The NC unit 7* exhibited erratic behavior at times and finally quit operating before the low dose rate calibration could be made. The NC units, as seen from a comparison of 6* and 8, behave in a manner similar to that of the "regular" units.

Table 5-2 $^{60}$Co Calibration Data for Dosimeters 1, 2, 3, and 4

| Actual Dose Rate, mrad/hr | Dosimeter 1 | | Dosimeter 2 | | Dosimeter 3 | | Dosimeter 4 | |
|---|---|---|---|---|---|---|---|---|
| | Time Between Pulses, sec | #mrad Pulse | Time Between Pulses, sec | #mrad Pulse | Time Between Pulses, sec | #mrad Pulse | Time Between Pulses, sec | #mrad Pulse |
| 64,110 | 0.54 | 9.62 | 0.53 | 9.44 | 0.161 | 2.87 | 0.711 | 12.66 |
| 34,340 | 1.02 | 9.72 | 1.032 | 9.84 | 0.287 | 2.74 | 1.28 | 12.21 |
| 20,960 | 1.64 | 9.55 | 1.69 | 9.84 | 0.474 | 2.76 | 2.07 | 12.05 |
| 13,800 | 2.44 | 9.34 | 2.48 | 9.51 | 0.700 | 2.68 | 3.21 | 12.31 |
| 9,725 | 3.42 | 9.23 | 3.43 | 9.27 | 0.983 | 2.66 | 4.56 | 12.32 |
| 7,235 | 4.53 | 9.11 | 4.60 | 9.25 | 1.29 | 2.59 | 5.86 | 11.78 |
| 1,231 | 25.8 | 8.82 | 26.8 | 9.16 | 7.29 | 2.49 | 34.1 | 11.66 |
| 727 | 43.5 | 8.78 | 44.5 | 8.99 | 12.1 | 2.44 | 56.4 | 11.39 |
| 339 | 91.9 | 8.65 | 95.0 | 8.95 | 25.2 | 2.37 | 119.8 | 11.28 |
| 260 | 121.2 | 8.75 | 126.5 | 9.14 | 32.4 | 2.34 | 160.1 | 11.56 |
| 179.06 | 171.9 | 8.55 | 199.1 | 9.93 | 52.1 | 2.59 | 250.1 | 12.44 |
| 78.57 | 388.5 | 8.48 | 439.3 | 9.59 | 114.3 | 2.50 | 562.6 | 12.28 |
| 38.71 | 821.2 | 8.83 | 898.6 | 9.66 | 219.2 | 2.36 | 1,130.2 | 12.15 |
| 19.65 | 1,474.8 | 8.05 | 1,649.0 | 9.00 | 414.2 | 2.27 | 2,027.5 | 11.07 |
| 7.872 | 3,731.7 | 8.16 | 4,325.6 | 9.46 | 1,007.8 | 2.20 | 5,208.0 | 11.39 |
| 4.47 | 5,653.7 | 7.02 | 6,302.9 | 7.83 | 1,574.0 | 1.95 | 7,896.7 | 9.81 |
| 2.003 | 12,419.4 | 6.91 | 14,002.9 | 7.79 | 3,444.4 | 1.92 | 16,886.0 | 9.40 |
| 1.034 | 22,560.9 | 6.48 | - | - | - | - | - | - |

Notes:
a. The data for dosimeter 1 was taken at a slightly higher (about 2%) dose rate, but the results have been normalized to compare with the others.
b. The calibration for 260mrad/hr and above was done using G-454 and G-2 was used for the lower rates. (see Appendix D)
c. The calibration times between pulses are averages over several pulses except for the long counts.
d. The temperature during the calibration was 25 ± 3°C.

Table 5-3 $^{60}Co$ Calibration Data for Dosimeters 5, 6*, 7*, and 8

| Actual Dose Rate, mrad/hr | Dosimeter 5 | | Dosimeter 6* | | Dosimeter 7* | | Dosimeter 8 | |
|---|---|---|---|---|---|---|---|---|
| | Time Between Pulses, sec | #mrad/Pulse | Time Between Pulses, sec | #mrad/Pulse | Time Between Pulses, sec | #mrad/Pulse | Time Between Pulses, sec | #mrad/Pulse |
| 64,110 | - | - | 0.280 | 4.99 | - | - | 0.55 | 9.80 |
| 34,340 | - | - | 0.509 | 4.86 | 2.5 | 23.85 | 1.025 | 9.78 |
| 20,960 | - | - | 0.818 | 4.76 | 5.23 | 30.45 | 1.68 | 9.78 |
| 13,800 | - | - | 1.20 | 4.60 | 6.3 | 24.15 | 2.50 | 9.58 |
| 9,725 | - | - | 1.64 | 4.43 | 6.77 | 18.29 | 3.42 | 9.24 |
| 7,235 | - | - | 2.18 | 4.38 | 20.15 | 40.50 | 4.56 | 9.17 |
| 1,231 | - | - | 12.3 | 4.21 | 68.1 | 23.29 | 25.8 | 8.82 |
| 727 | - | - | 20.4 | 4.12 | 113.9 | 23.00 | 42.9 | 8.66 |
| 339 | - | - | 43.1 | 4.06 | 198.3 | 18.67 | 89.7 | 8.45 |
| 260 | - | - | 57.6 | 4.16 | 284.4 | 20.54 | 117.7 | 8.50 |
| 179.06 | - | - | 84.9 | 4.22 | - | - | 182.7 | 0.09 |
| 78.57 | - | - | 181.9 | 3.97 | - | - | 411.8 | 8.98 |
| 38.71 | - | - | 353.5 | 3.80 | - | - | 812.4 | 8.74 |
| 19.65 | - | - | 611.6 | 3.34 | - | - | 1,468.1 | 8.01 |
| 7.872 | - | - | 1,554.8 | 3.40 | - | - | 3,581.3 | 7.83 |
| 4.47 | - | - | 2,395.9 | 2.98 | - | - | 5,647.7 | 7.01 |
| 2.003 | - | - | 5,067.6 | 2.82 | - | - | 12,444.5 | 6.92 |
| 1.034 | - | - | 8,745.7 | 2.51 | - | - | 20,790.2 | 5.97 |

Notes:
a. Dosimeter 5 was not in operation at the time of the calibration tests.
b. Dosimeter 7* did not operate properly after the high dose rate calibration.
c. The calibration for 260mrad/hr and above was done using G-454 and G-2 was used for the lower rates. (See Appendix D)
d. The calibration times between pulses are averages over several pulses except for the long counts.
e. The temperature during the calibration was 27 ± 5°C.

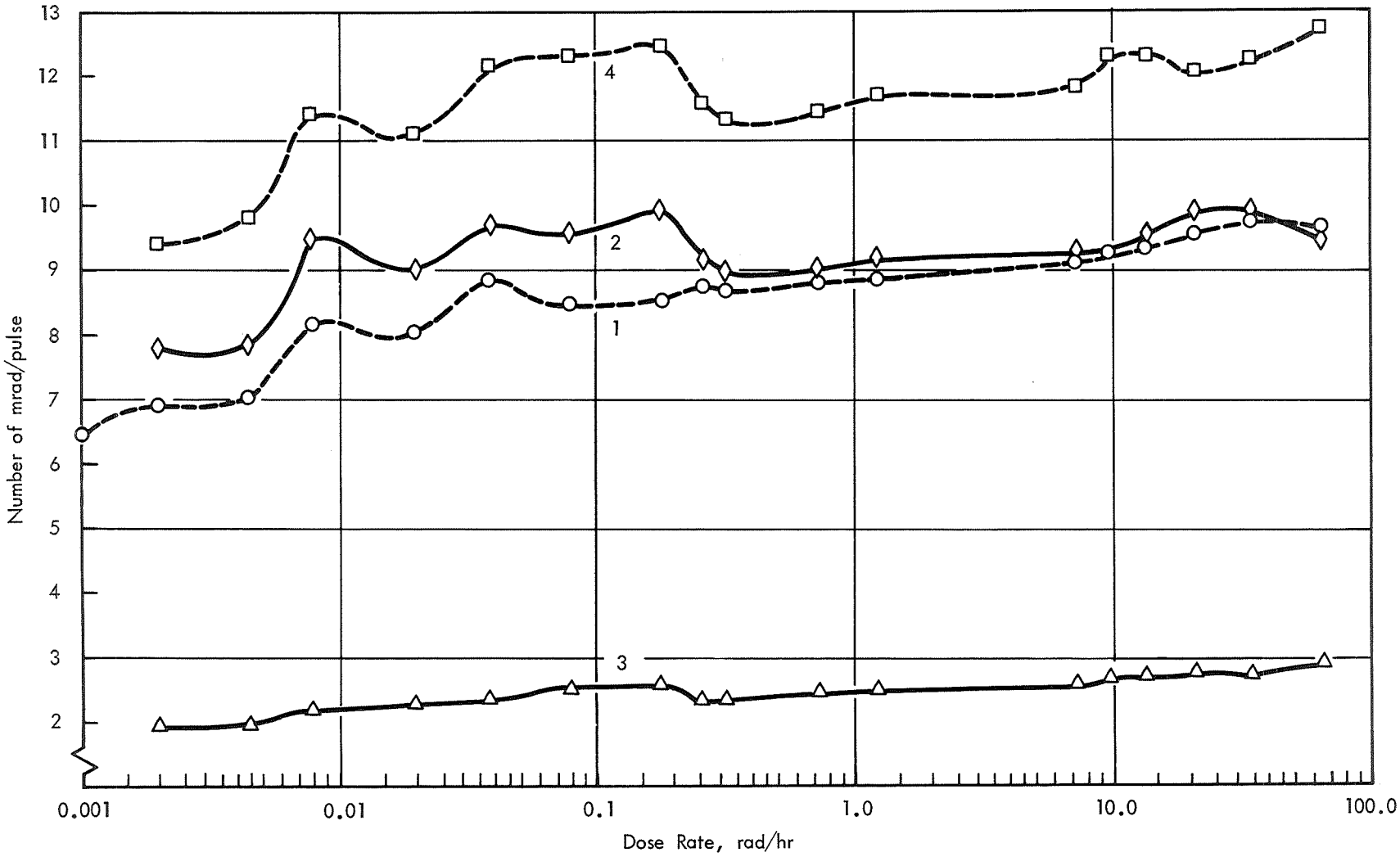


Figure 5-6 $^{60}$Co Calibration Results for Dosimeters 1,2,3, and 4

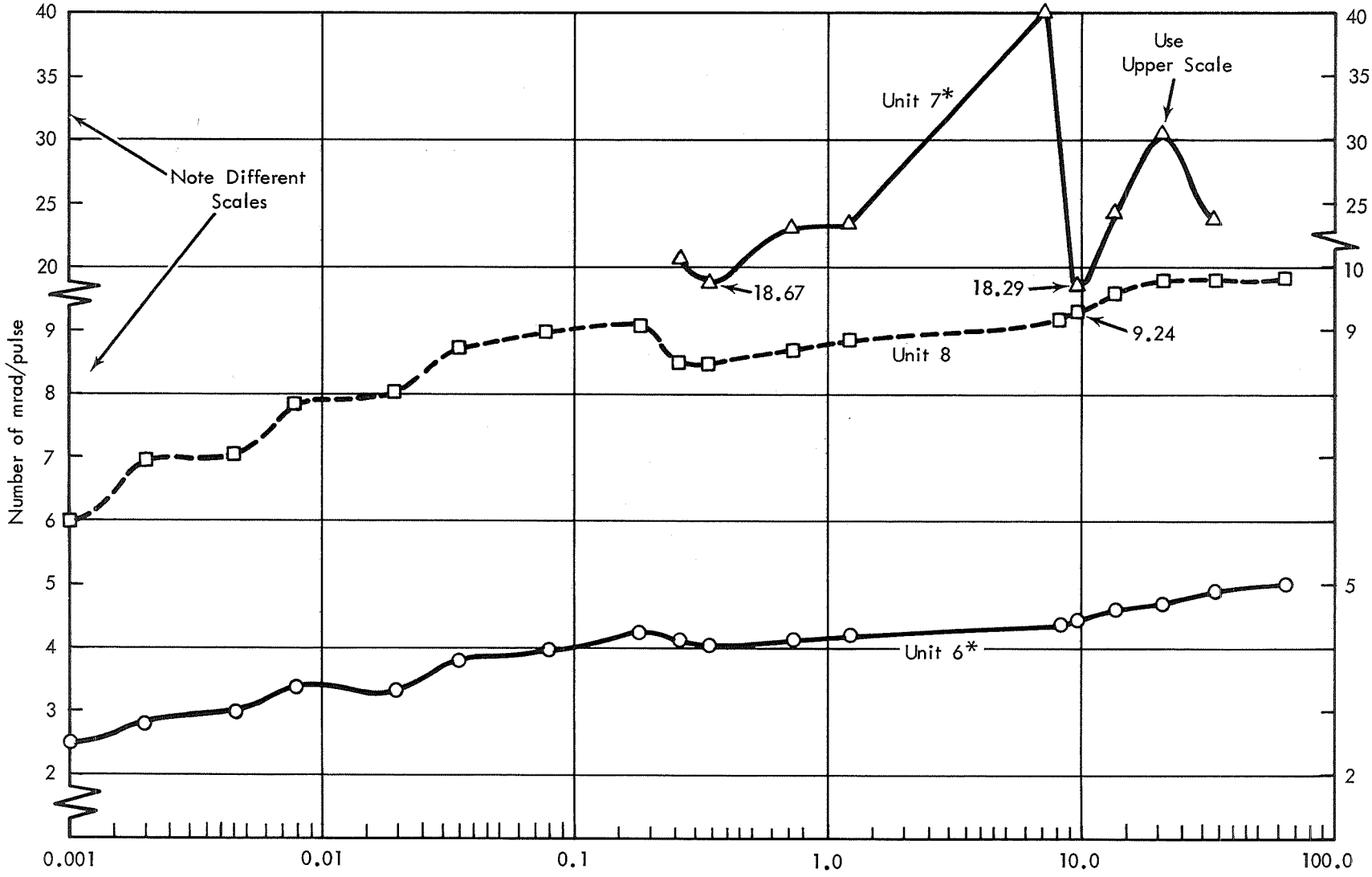


Figure 5-7 $^{60}$Co Calibration Results for Dosimeters 6,* 7,* and 8

The calibration data can be displayed in another manner which may be more informative to some readers. A fixed value of the absorbed dose per pulse can be selected and the deviation from this value plotted versus the true dose rate. This has been done for the collected data and the percentage-wise results are tabulated in Table 5-4 and some are plotted in Figure 5-8. These results show that the detected tissue equivalent dose is within about 10% of the true dose over a range of more than four decades of dose rate for the majority of the dosimeters tested. Again, background radiation probably caused the large discrepancies at the low dose rates. Dosimeters 3 and 6* show a larger percentage deviation from the true dose than the others, but it should be noted that their values of absorbed dose per pulse are much smaller than that of the other dosimeters tested.

## 5.4 Temperature Effects

The tests to determine temperature effects on the dosimeters were performed inside a Tenney-mite environmental chamber using the G-2 $^{60}Co$ source located above the units along line CD as shown in Figure 5-3. The dose rates in the experimental configuration used are not well known enough to convert the time between pulses to dose per pulse, but the approximate dose rates are indicated for the time-temperature data shown in Figures 5-9 and 5-10.

The test of dosimeter 5 was started at 70°F and data was taken for several temperatures up through 180°F. After cooling again to 70°F, the unit operated briefly and then quit. Examination of the unit did not give any clues as to the cause of the failure.

Table 5-4

Deviation of Dose/Pulse from a Selected Value

| Dosimeter | 1 | 2 | 3 | 4 | 6* | 8 |
|---|---|---|---|---|---|---|
| Selected Value of #mrad/pulse | 9.00 | 9.00 | 2.50 | 12.00 | 4.00 | 9.00 |
| Dose Rate, mrad/hr | % Deviation of $\frac{\#mrad}{pulse}$ from Selected Value[1] | | | | | |
| 64,110 | 6.9 | 4.9 | 14.8 | 5.5 | 24.8 | 8.9 |
| 34,340 | 8.0 | 9.3 | 9.6 | 1.7 | 21.5 | 8.7 |
| 20,960 | 6.1 | 9.3 | 10.4 | 0.4 | 19.0 | 8.7 |
| 13,800 | 3.8 | 5.7 | 7.2 | 2.6 | 15.0 | 6.4 |
| 9,725 | 2.6 | 3.0 | 6.8 | 2.7 | 10.8 | 2.7 |
| 7,235 | 1.2 | 2.8 | 3.6 | -1.8 | 9.5 | 1.9 |
| 1,231 | -2.0 | 1.8 | -0.4 | -2.8 | 5.3 | -2.0 |
| 727 | -2.4 | -0.1 | -2.4 | -5.1 | 3.0 | -3.8 |
| 339 | -3.9 | -0.6 | -5.2 | -6.0 | 1.5 | -6.1 |
| 260 | -2.8 | 1.6 | -6.4 | -3.7 | 4.0 | -5.6 |
| 179.06 | -5.0 | 10.3 | 3.6 | 3.7 | 5.5 | 1.0 |
| 78.57 | -5.8 | 6.6 | 0.0 | 2.3 | -0.8 | -0.2 |
| 38.71 | -1.9 | 7.3 | -5.6 | 1.2 | -5.0 | -2.9 |
| 19.65 | -10.5 | 0.0 | -9.2 | -7.7 | -16.5 | -11.0 |
| 7.872 | -9.3 | 5.1 | -12.0 | -5.1 | -15.0 | -13.0 |
| 4.47 | -22.0 | -13.0 | -22.0 | -18.2 | -25.5 | -22.1 |
| 2.003 | -23.2 | -13.4 | -23.2 | -21.7 | -29.5 | -23.1 |

[1] Sample calculation of deviation for dosimeter 1 at 64,110 mrad/hr:

$$\text{Deviation} = \frac{9.62-9.00}{9.00} \times 100 = 6.9\%$$

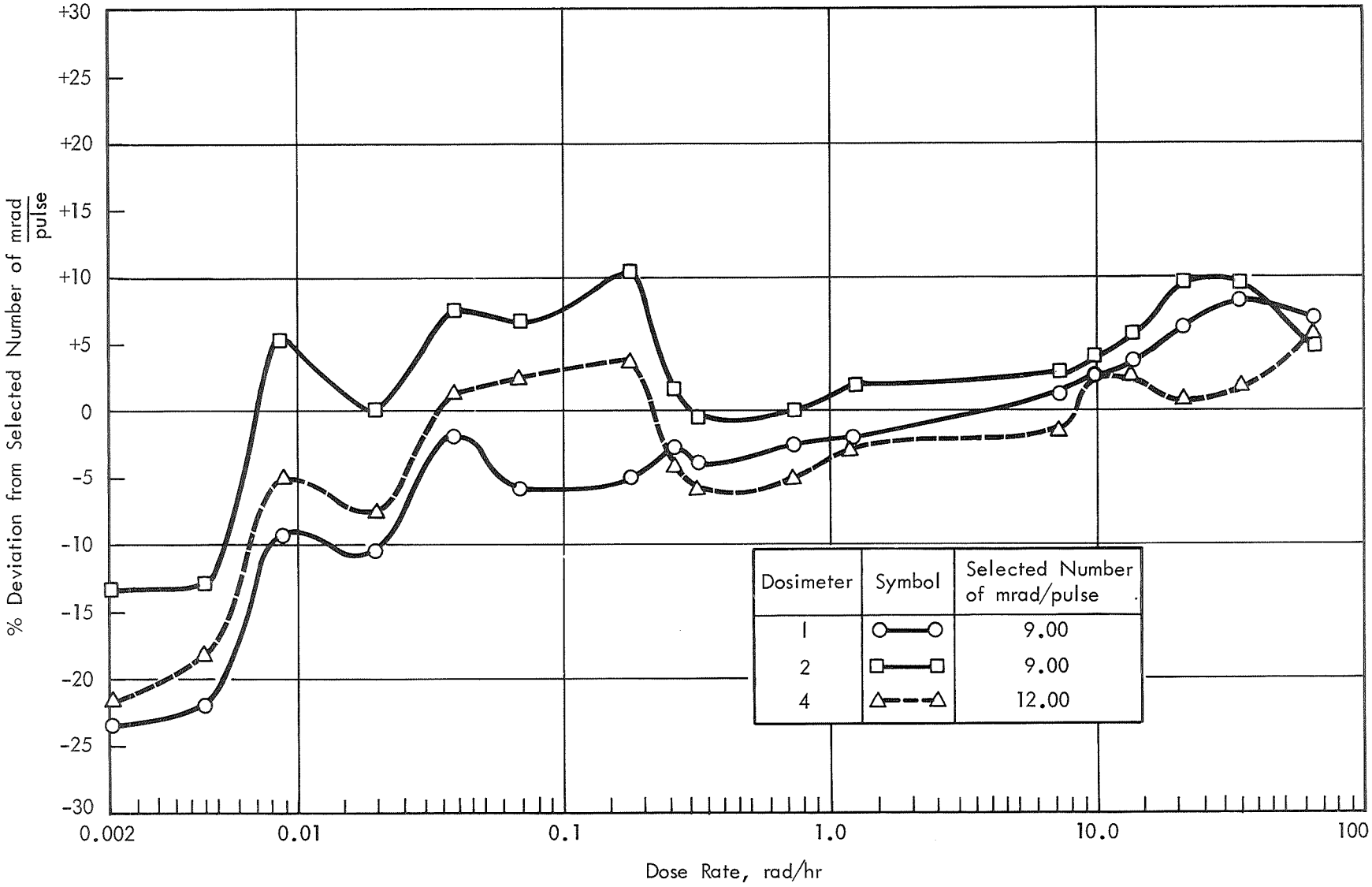


Figure 5-8 Deviation of Dose/Pulse From Selected Value for Dosimeters 1, 2, and 4

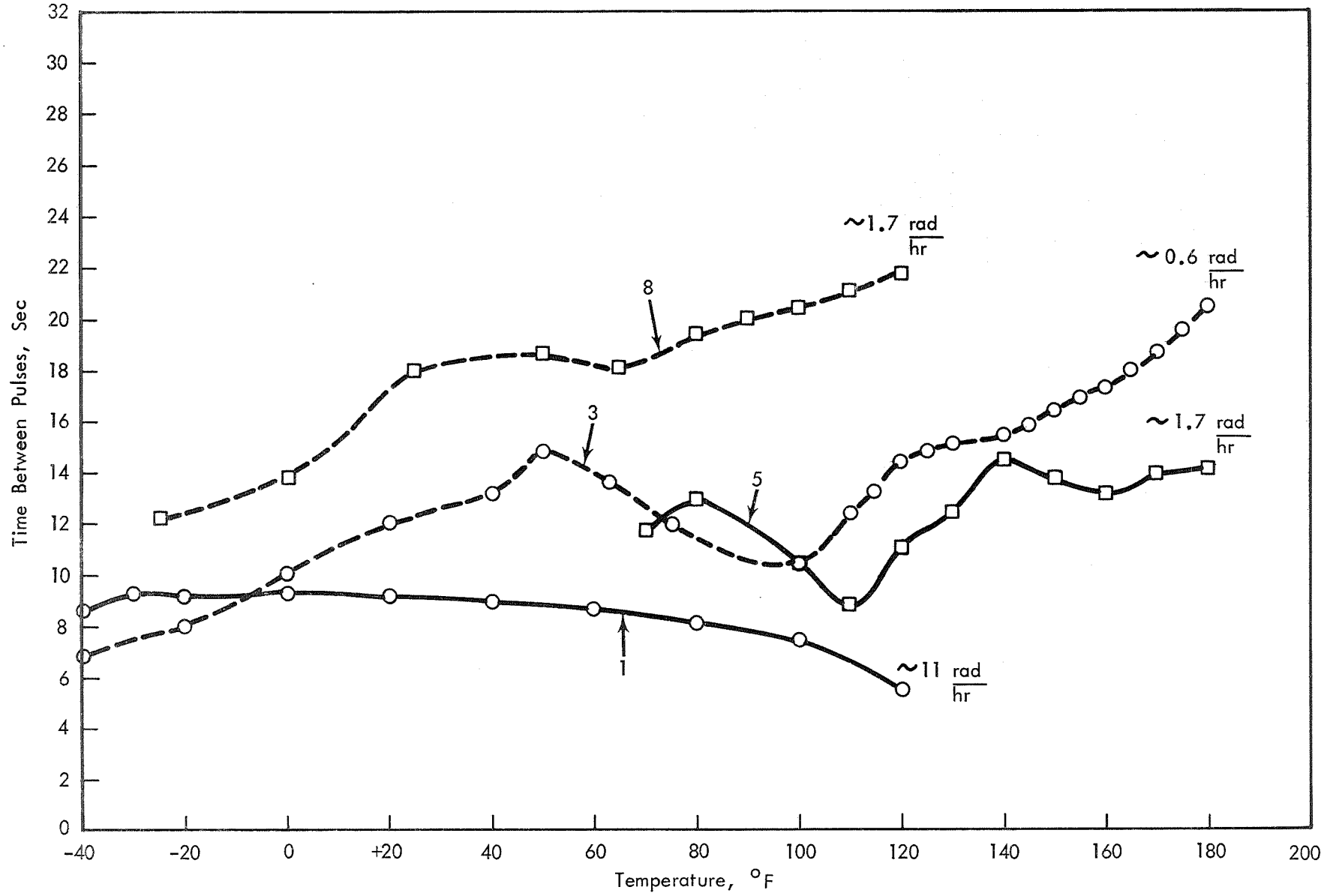


Figure 5-9 Temperature Data for Dosimeters 1,3,5, and 8

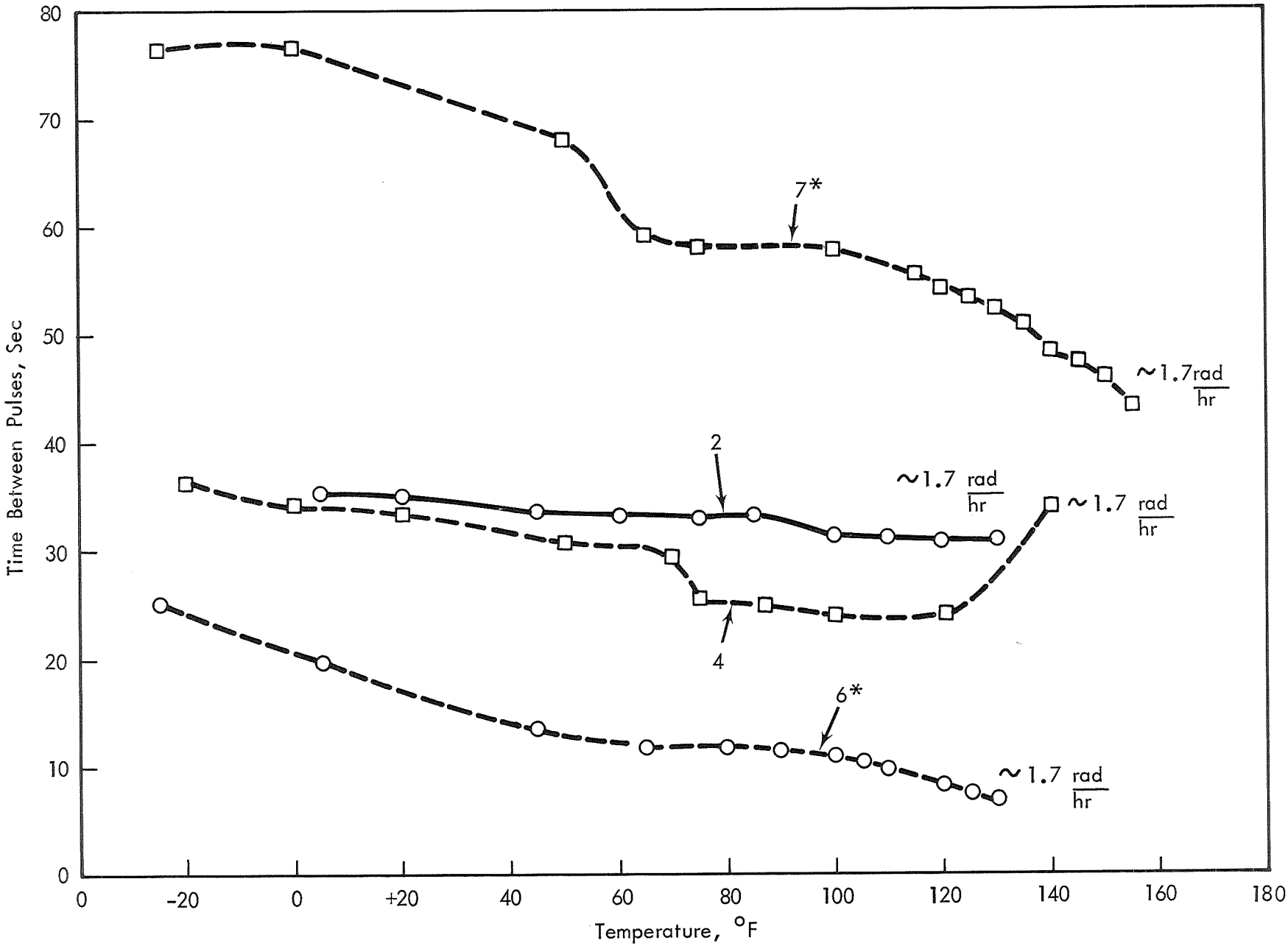


Figure 5-10 Temperature Data for Dosimeters 2, 4, 6,* and 7*

The overall variation of the time between pulses with temperature is represented by the data in Table 5-5.

Table 5-5 Slope of the Temperature Dependence

| Dosimeter | Approximate Overall Slope, sec/pulse-F° | |
|---|---|---|
| 1 | -0.02 | 0.0 ± 0.06 |
| 2 | -0.03 | |
| 3 | +0.06 | |
| 4 | -0.05 | |
| 5 | +0.02 | |
| 8 | +0.06 | |
| 6* | -0.13 | NC type |
| 7* | -0.20 | |

The NC units exhibit a relatively strong negative slope. The result is that at higher temperatures, there is less time between pulses at constant dose rates. In other words, the necessary amount of radiation collected to cause a pulse is less at higher temperatures. The "regular" units exhibit much weaker dependence, but in both directions.

A partial explanation can be reasoned by saying that the NC unit fibers become more elastic at higher temperatures and thus take less force (proportional to charge collected which is, in turn, proportional to the integrated dose) and consequently less time to cause a pulse to occur. By the same token, however, the fibers in the "regular" units also become more elastic. The fibers are in tension against the rods and whether or not they take more or less force to

be pushed away depends on how elastic they become, the fiber length, and the tension. Depending on these factors, the fiber will have to be bent either more or less at elevated temperature to break contact with the rod.

It should be mentioned that these temperature dependencies do not become significant until high dose rates at extreme temperatures are encountered. For instance, using the largest slope calculated, the difference in the number of millirads/pulse (taking 10 as the normal value) for a temperature difference of 50°F and at a dose rate of 1 rad/hr is about 28%.

## 5.5 Vibration and Shock

Dosimeter 1 was subjected to the simulated mission vibration and shock tests specified by NASA-MSC for their space qualified radiation detection instruments. The dosimeter was tested using the G-367 $^{137}Cs$ source and its operation after the simulation tests is essentially the same as it was before they were performed. (refer to Table 5-6)

Table 5-6

Comparison of Data Taken Before and After the Mission Vibration and Shock Tests

| Number of Pulses Averaged | Average Time Between Pulses, sec | | |
|---|---|---|---|
| | Before Tests | After Part of Tests | After All Tests |
| 10 | 26.8 | 27.5 | 26.5 |

## 5.6 Gas Leak Tank

The QFE dosimeters are filled to a pressure of 760 Torr (i.e. 1 atm.) with ethylene. Dosimeter 1 was tested for gas leaks with a Veeco MS-12 leak detector. The leak rate was found to be $1.8\ (10^{-10})$ atm-cc/sec (He) which is only about 20% above the background reading.

# VI. SUMMARY AND CONCLUSIONS

The major accomplishments of this work are summarized below:

1. Theoretical considerations to point out trends in intrinsic behavior were formulated to aid in the design and sizing of the quartz fiber electrometer.

2. Small automatic recycling quartz fiber electrometers were designed, developed, and constructed.

3. Tissue equivalent ionization chambers for use with the quartz fiber electrometers were designed and built.

4. The quartz fiber electrometer dosimeter systems, complete with the pulse shaping electronics, were tested to determine their applicability for use as space qualified radiation detection instruments.

As a result of this dosimeter study, the following conclusion is drawn:

1. The performance of the dosimeters in the tests conducted (i.e. orientation, high and low dose rate $^{60}Co$ calibration, temperature, vibration and shock, and gas leak) indicates that they can indeed be developed into meritous space qualified radiation dosimeters.

# VII. RECOMMENDATIONS FOR FURTHER INVESTIGATION

In view of the findings of this study, the following suggestions are made for future work on quartz fiber electrometer dosimeter systems:

1. Methods to accurately control and select the fiber diameter should be employed.

2. The Signa-Kote coating on the quartz fibers should be made as perfectly uniform as possible.

3. New methods of attaching the fibers to their support rods should be considered.

4. It should be determined whether or not the application of a base coat of metal on the quartz rod before gold deposition will significantly enhance the electrometer performance.

5. The quantitative effect of ethylene pressure variation should be determined.

6. The dosimeter response to alpha, beta, and proton radiation should be measured.

7. It should be determined which type of electrometer, NC or "regular", can be most predictably constructed.

8. Although it is suspected that almost any value between about 1 and 100 mrad/pulse is feasible, all factors influencing the control and adjustment of the absorbed dose per pulse should be investigated to determine the practical limitations.

9. Consideration should be given to the development of a self-contained dosimeter system complete with radiation detection element, battery pack, electronics package, electroluminescent digital display, and anodized aluminum case.

## APPENDIX A

## TISSUE EQUIVALENT ION CHAMBER

It has been indicated [15] that tissue equivalence depends on the materials used in the ion chamber having the same number of electrons per unit volume as tissue. This number, for a given substance, is proportional to the ratio of the atomic number of the mass number (i.e. Z/A).

The elements composing human muscle tissue and their weight percentages have been presented in the literature[16]. The total Z number is given as 55.087. The A number calculation is shown in Table A-1.

Table A-1 Total Mass Number of Human Muscle Tissue

| Element | Weight % | Atomic Weight | A |
|---|---|---|---|
| C | 1.024 | 12.011 | 12.299 |
| H | 10.2 | 1.008 | 10.282 |
| O | 4.556 | 16.0 | 72.896 |
| N | 0.25 | 14.008 | 3.502 |
| Na | 0.0036 | 22.991 | 0.081 |
| Mg | 0.0008 | 24.32 | 0.020 |
| P | 0.0065 | 30.975 | 0.021 |
| S | 0.0156 | 32.066 | 0.500 |
| K | 0.0077 | 39.1 | 0.301 |
| Ca | 0.00017 | 40.08 | 0.007 |

Effective A = 99.901

The (Z/A) values for muscle tissue, Delrin, and ethylene are very near one another as seen in Table A-2.

Table A-2 (Z/A) Values for Tissue, Delrin, and Ethylene

| Substance | Tissue | Delrin $(CH_2O)_n$ | Ethylene $(C_2H_4)$ |
|---|---|---|---|
| Z/A | 0.551 | 0.533 | 0.571 |

Additional testimony to Delrin being a good tissue equivalent material is that the attenuation and absorption coefficients are very close to one another. (This actually stems from the similarity of (Z/A) values.) The numbers [17] in Table A-3 show the proximity of these coefficients:

Table A-3 Attenuation and Absorption Coefficients of Delrin & Tissue

| Photon Energy (MeV) | Attenuation Coefficient ($cm^2/g$) | | Absorption Coefficient ($cm^2/g$) | |
|---|---|---|---|---|
| | Tissue | Delrin | Tissue | Delrin |
| 0.010 | 5.2582 | 3.9928 | 4.8412 | 3.6009 |
| 0.050 | 0.2211 | 0.2065 | 0.0295 | 0.0315 |
| 0.100 | 0.1698 | 0.1636 | 0.0251 | 0.0236 |
| 0.500 | 0.0957 | 0.0928 | 0.0326 | 0.0316 |
| 1.000 | 0.0700 | 0.0678 | 0.0307 | 0.0297 |
| 5.000 | 0.0299 | 0.0289 | 0.0191 | 0.0184 |
| 10.000 | 0.0216 | 0.0209 | 0.0158 | 0.0152 |
| 50.000 | 0.0160 | 0.0152 | 0.0146 | 0.0139 |
| 100.000 | 0.0165 | 0.0157 | 0.0158 | 0.0150 |

On the basis of the above presented material, the Delrin-ethylene system is said to be tissue equivalent.

## APPENDIX B

## STOPPING POWER CALCULATION

The $\rho$ in the Bragg-Gray theory is the mass stopping power ratio.

$$\rho = \frac{\text{mass stopping power of medium}}{\text{mass stopping power of gas}}$$

There are published formulas by which $\rho$ may be calculated when the medium and the gas are known. The following table lists the results of calculations for ethylene gas and a Delrin medium.

Table B-1 Mass Stopping Power Ratio Using Delrin and Ethylene

| Electron Energy, Mev | $\rho$ | Reference |
|---|---|---|
| 0.1 | 0.899 | 18 |
| 1.0 | 0.910 | |
| 0.1 | 0.900 | 19 |
| 1.0 | 0.908 | |
| 0.1 | 0.899 | 20 |
| 1.0 | 0.907 | |

Average = 0.904

# APPENDIX C

## PHYSICAL PROPERTIES OF MATERIALS USED IN THE QFE DOSIMETER SYSTEM

### 1. Quartz (Ref. 21)

| Property | Value |
|---|---|
| Density | 2.2g/cc |
| Hardness | 4.9Mhos |
| Tensile Strength | 7,000 psi |
| Compressive Strength | >160,000 psi |
| Bulk Modulus | $\sim 5.3(10^6)$ psi |
| Rigidity Modulus | $4.5(10^6)$ psi |
| Young's Modulus | $10.4(10^6)$ psi* |
| Poisson's Ratio | 0.16 |
| Thermal Conductivity | 0.0033 cal/sec-cm-°C |
| Specific Heat | 0.18 cal/g |
| Softening Point | ~1665°C |
| Coefficient of Thermal Expansion...(avg.) | $5.5(10^{-7})°C^{-1}$ (20°C-320°C) |
| Annealing Point | ~1140°C |
| Strain Point | 1070°C |
| Electrical Resistance | 9.5 $\log_{10}R$ for $cm^3$ at 350°C |
| Dielectric Constant | 3.75 at 20°C, 1 mc |
| Dielectric Loss Factor | <0.0004 at 20°C, 1 mc |
| Index of Refraction | 1.4585 |

### 2. Ethylene (Ref. 22)

| | |
|---|---|
| Synonym | Ethene ($C_2H_4$) |
| Family | Olefin Hydrocarbon of Alkene Family |
| Molecular Weight | 28.05 |
| Boiling Point (1 atm.) | -154.66°F (-103.7°C) |
| Freezing Point (1 atm.) | -273.1°F (-169.5°C) |
| Specific Gravity, Air = 1 | 0.978 |
| Critical Temperature | 48.65°F (9.25°C) |
| Critical Pressure | 735 psia (50 atm.) |
| Critical Density | 0.288g/cc |
| Thermal Conductivity, 32°F | 0.0101 BTU-in./hr-$ft^2$-°F |
| $C_p$; 15°C, 1 atm | 0.3592 cal/g-°C |
| $C_v$; 15°C, 1 atm | 0.2858 cal/g-°C |
| Flammable Limits in Air | 3.1-32.0% (by volume) |
| Autoignition Temperature | 1009°F |
| Viscosity; gas, 15°C | 0.0099 centipoise |

* Refer to Section 2.1.4

### 3. Delrin (Ref. 23)

| Property | Value |
|---|---|
| Formula | $n\text{-}CH_2O$ |
| Melting Point | 347°F |
| Specific Heat | 0.35 BTU/lb-°F |
| Thermal Conductivity | 1.6 BTU-in./hr-ft$^2$-°F |
| Specific Gravity | 1.40-1.42 |
| Poisson's Ratio | 0.35 |
| Surface Resistivity | $>10^{16}$ohms |
| Coefficient of Linear Thermal Expansion | $4.2(10^{-5})°F^{-1}$(-40 to +85°F)<br>$5.0(10^{-5})°F^{-1}$(+85 to +140°F)<br>$5.5(10^{-5})°F^{-1}$(+140 to +220°F) |
| Dielectric Strength | 5,870 volts/mil @ 1.2 mils thick<br>1,210 volts/mil @ 20 mils thick<br>590 volts/mil @ 73 mils thick |
| Dielectric Constant (73°F, 50% R.H.) | 3.74 ($10^2$cps)<br>3.71 ($10^4$cps)<br>3.69 ($10^6$cps) |

### 4. Aluminum (Ref. 24)

| | |
|---|---|
| Type | 6061 |
| Composition | 1.0%Mg<br>0.25%Cu<br>0.60%Si<br>0.25%Cr<br>97.9%Al |
| Specific Gravity | 2.70 |
| Density | 0.098 lb/in$^3$ |
| Melting Range | ~1080-1205°F |
| Electrical Conductivity | 40 (% of Cu) |
| Thermal Conductivity (25°C) | 0.37 CGS units |
| Average Coefficient of Thermal Expansion | $12.0(10^{-6})°F^{-1}$(-76°F to + 68°F)<br>$13.1(10^{-6})°F^{-1}$(+68°F to 212°F) |

APPENDIX D

## DOSE vs. DISTANCE DATA FOR RADIATION SOURCES USED IN THE EXPERIMENTS

The dose rates at various distances from the gamma sources used in the experiments are presented in this appendix. The sources are identified in Table D-1 and the graphed information follows in Figures D-1, D-2, and D-3.

Table D-1 Source Identification

| Item | Source Designation | | |
|---|---|---|---|
| | G-2 | G-367 | G-454 |
| Type | $^{60}Co$ | $^{137}Cs$ | $^{60}Co$ |
| Gamma Energy, Mev | 1.17,1.33 | 0.662 | 1.17,1.33 |
| Use | Temperature, Test, Low Dose Rate Calibration | Orientation Test, Saturation Voltage Test | High Dose Rate Calibration |
| Comment | 1/4"d x 3/4" SS capsule | 3/8"d x 3/8" br. screw in 30" Al rod | Health Physics Well Source |

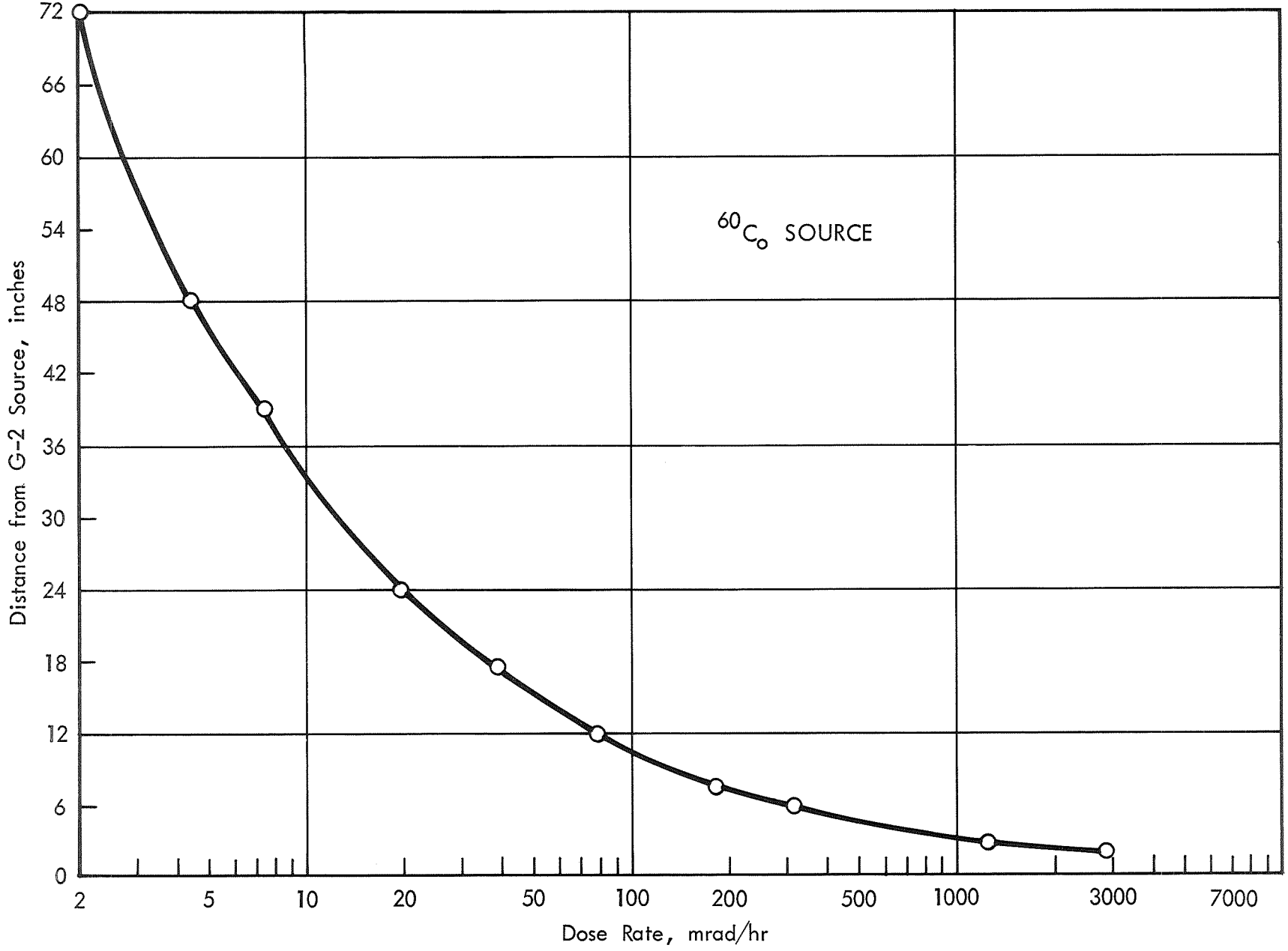


D-1 Dose Rate vs. Distance for G-2 Source

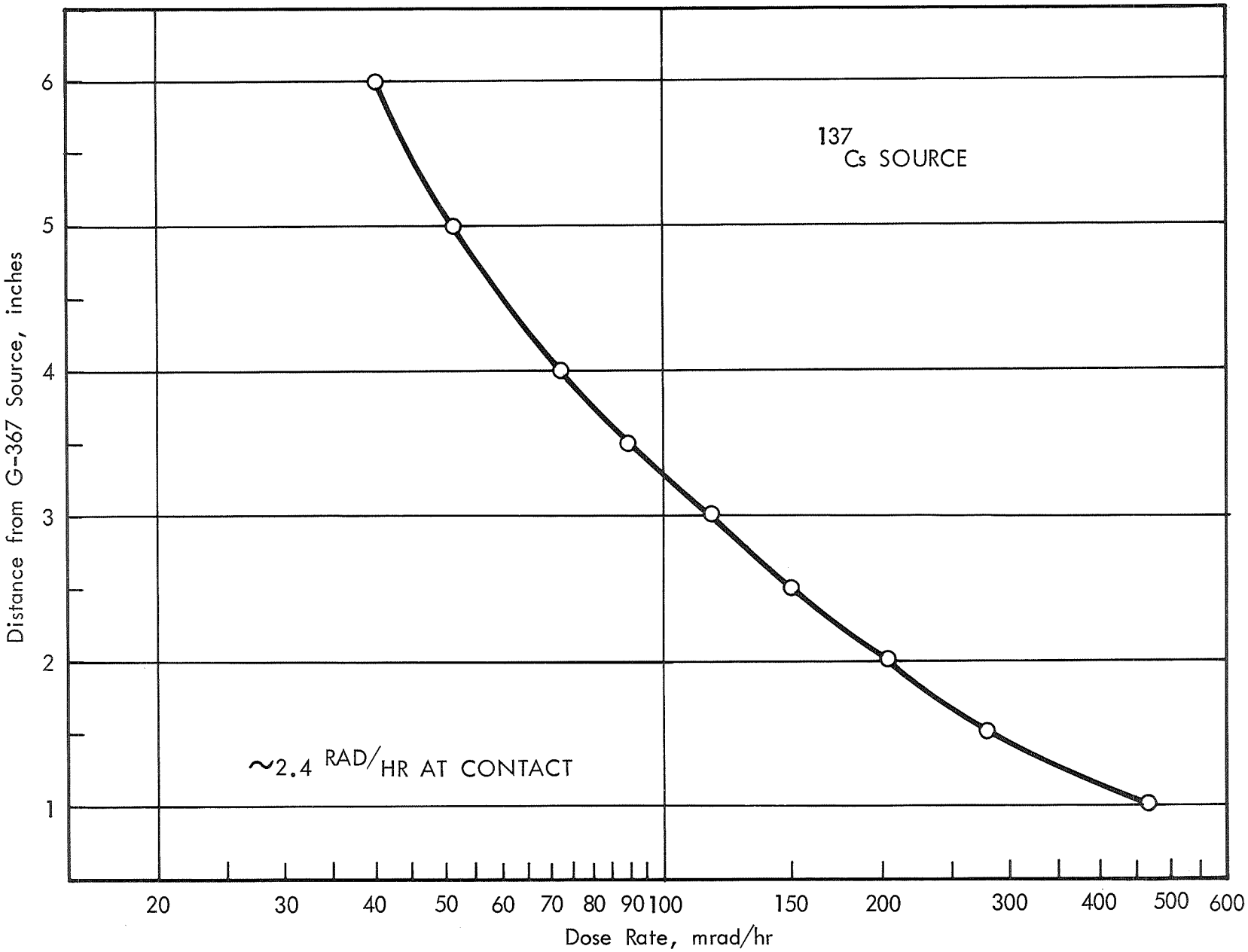


D-2 Dose Rate vs. Distance for G-367 Source

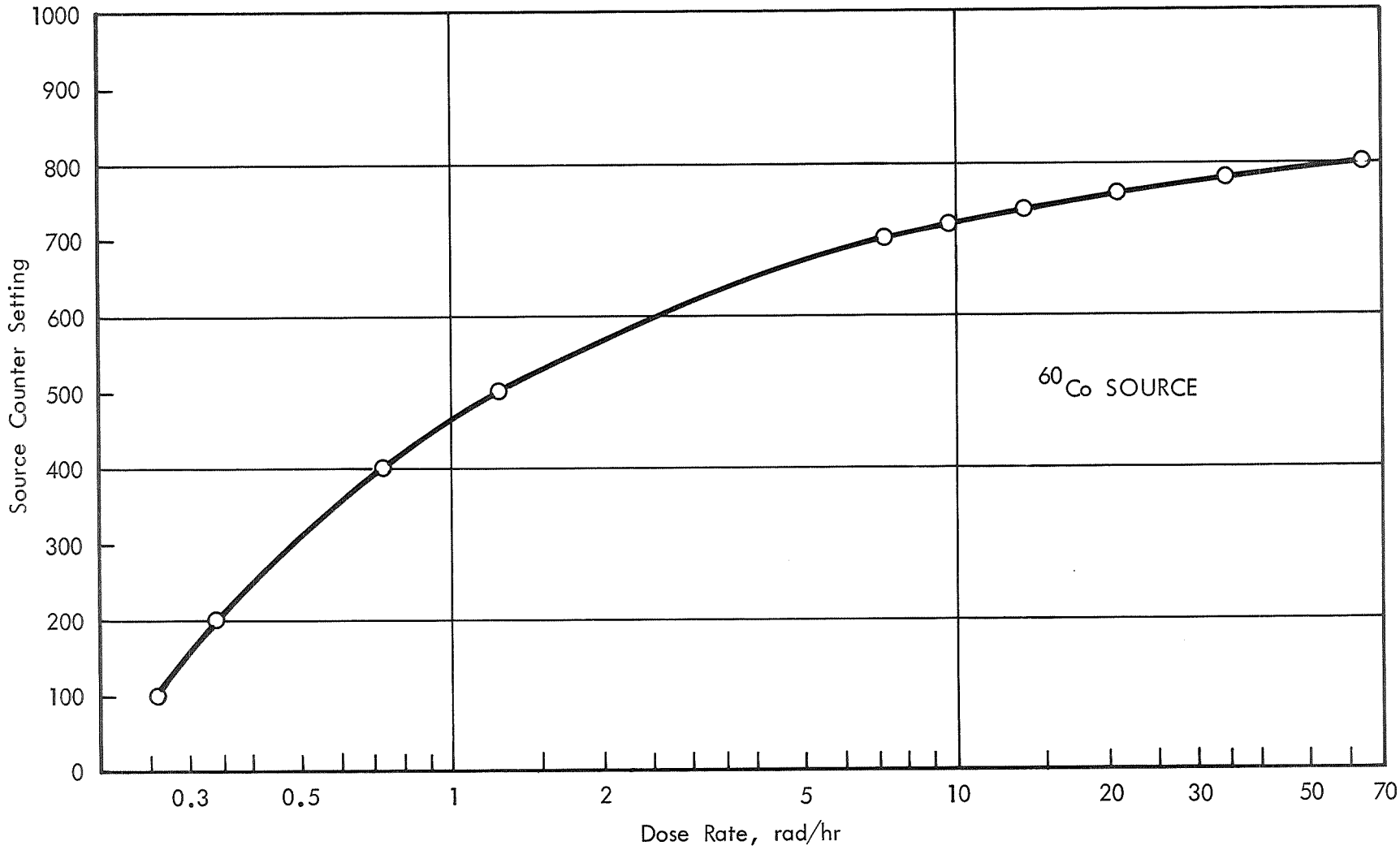


D-3 Dose Rate vs. Source Counter Setting for G-454

REFERENCES


1. Lauritsen, C. C., and Lauritsen, Thomas, "A Simple Quartz Fiber Electrometer," Rev. Sci. Instr., 8, 438 (1937).

2. Neher, H. V., "An Automatic Ionization Chamber," Rev. Sci. Instr., 24, 2, 99 (1953).

3. Johnston, Alan R., and Neher, H. V., "Modification to the Automatic Ionization Chamber," Rev. Sci. Instr., 27, 173 (1956).

4. Neher, H. V., "Variable Sensitivity Automatic Ionization Chamber," Rev. Sci. Instr., 32, 1, 48 (1961).

5. Hosemann, Rolf, and Warrikhoff, Harold, F. H., "Self-Powered Dosimeter for Gamma and X-Radiation," Nucleonics, 22, 3, 51 (1964).

6. Adams, R. J., "The Use of Gold Coated Quartz Fibers in High Pressure Propostional Counters," Nucl. Instr. Methods, 57, 351 (1967).

7. Johnston, Alan R., and Neher, H. V., "Techniques Useful in Evacuating and Pressurizing Metal Chambers," Rev. Sci. Instr., 25, 517 (1954).

8. Miles, Ralph F., "Density of Cosmic-Ray Neutrons in the Atmosphere," J. Geophys. Res., 69, 7, 1277 (1964).

9. Kirk, Paul L., and Schaffer, F. L., "Construction and Special Uses of Quartz Helix Balances," Rev. Sci. Instr., 19, 11, 785 (1948).

10. Drew, C. M. and Ernsberger, F. M., "Improvements in Design and Construction of Quartz Helix Balances," Rev. Sci. Instr., 24, 2, 117 (1953).

11. Hemenway, Curtis L., and Patashnick, Harvey, "Oscillating Fiber Microbalance," Rev. Sci. Instr., 40, 8, 1008 (1969).

12. Neher, H. V., in Procedures in Experimental Physics, Strong,J., ed., pp. 188-216, Prentice-Hall, Inc., New York, (1938).

13. Craig, Roderick, and Kirk, Paul L., "Reproducible Construction of Quartz Fiber Devices," Rev. Sci. Instr., 19, 11, 777 (1948).

14. Fletcher, C., and Wiley, Ralph, "Development of a Flight-Qualified Whole Body Socimeter System," FZK-258, pp. 85-90, General Dynamics/Fort Worth (1965).

15. Dainty, J., CRM-482, May 17, 1950.

16. Shonka, F. R., Rose, J. E., and Failla, G., Proc. 2nd U.N. Int. Conf. Peaceful Uses At. Energy, 21, 184-187 (1958).

17. "X-Ray Absorption in Dose Equated Materials," p. 61, Tech. Report No. WL-TR-64-134.

18. Hine, G. J., and Brownell, G. L., eds., Radiation Dosimetry, Chapter 1, Academic Press, New York, (1956).

19. Evans, Robley D., The Atomic Nucleus, Chapter 22, McGraw-Hill, New York, 11th printing, (1967).

20. "Stopping Powers for Use With Cavity Chambers," NBS Handbook 79, (1961).

21. The Chemical Rubber Company, eds., Handbook of Chemistry and Physics, 49th ed., (1969).

22. Matheson Gas Data Book, p. 195, The Matheson Company, Inc., 1961.

23. Delrin Information Sheet, A-63463, DuPont, November, 1968.

24. Miner, D. F., and Seastone, J. B., eds., Handbook of Engineering Materials, John Wiley and Sons, Inc., (1955).